Computer-Aided Design of

Low Noise Microwave Circuits

Thesis by

Scott William Wedge

In Partial Fulfillment of the Requirements

for the Degree of

Doctor of Philosophy

California Institute of Technology

Pasadena, California

1991

(Submitted May 23, 1991)

To Cindy, with Love

Acknowledgements

It is a pleasure to acknowledge my advisor David Rutledge for his guidance, support, and abundant encouragement given over the years. His energy and enthusiasm have been contagious, and have made my stay at Caltech a stimulating experience.

Thanks go to Hughes Aircraft Company, in general, for being a source of continued financial support through their doctoral fellowship program. Thanks go, in particular, to members of the RF Technology Department for tolerating my stochastic work schedule, and for listening to many wild ideas.

I am grateful for the friendship, good conversation, and technical advice given by past and present members of the Caltech MMIC group. Namely, Kent Potter, Moonil Kim, Jon Hacker, Yong Guo, Zoya Popović, Gabriel Rebeiz, Rick Compton, and Karen Lee. Extra appreciation goes to Wyman Williams for his good counsel and TEXpertise, to office mates Bobby Weikle and Victor Lubecke for often sharing their guitars, and to Phil and Tricia Stimson for too often sharing their apartment for group and bridge-night activities. New members Mike DeLisio, David Haub, and J.C. Chiao are to be thanked for the vigor they have added to the group. Additional gratitude goes to Dale Yee and Mark Vaughan for all their help on the *PUFF* project, and to Dale for assistance on many other matters.

Finally, with unequaled gratefulness, I thank my wife Cindy and our families for tolerating my long absences, inattention, and cross country treks in the pursuit of higher education. Their love and encouragement shall not be forgotten.

Computer-Aided Design of

Low Noise Microwave Circuits

Abstract

Devoid of most natural and manmade noise, microwave frequencies have detection sensitivities limited by internally generated receiver noise. Low-noise amplifiers are therefore critical components in radio astronomical antennas, communications links, radar systems, and even home satellite dishes. A general technique to accurately predict the noise performance of microwave circuits has been lacking. Current noise analysis methods have been limited to specific circuit topologies or neglect correlation, a strong effect in microwave devices. Presented here are generalized methods, developed for computer-aided design implementation, for the analysis of linear noisy microwave circuits comprised of arbitrarily interconnected components. Included are descriptions of efficient algorithms for the simultaneous analysis of noisy and deterministic circuit parameters based on a wave variable approach. The methods are therefore particularly suited to microwave and millimeter-wave circuits. Noise contributions from lossy passive components and active components with electronic noise are considered. Also presented is a new technique for the measurement of device noise characteristics that offers several advantages over current measurement methods.

Contents

Chapter 1

Introduction

Microwave frequencies occupy a portion of the electromagnetic spectrum that possesses an unusual quality. Lower frequencies are plagued by urban, galactic, solar and atmospheric noise, while higher frequencies suffer from atmospheric attenuation. In the microwave band, falling between 300 MHz and 30 GHz, nearly every type of natural and manmade noise is absent. This low-noise nature permits the detection of very faint signals; a tremendous advantage for the wireless transmission and/or reception of energy. Exploitation of this property has led to successful terrestrial, satellite and deep-space communications, ultra-sensitive radio astronomy, and accurate radar detection, tracking, and guidance.

In order to take full advantage of the noise absence at microwave frequencies, receivers require front-end amplifiers that contribute little of their own noise. In recent years, a considerable amount of research has been pursued specifically toward the development of microwave and millimeter-wave transistors with improved noise performance [1]. A summary of the current state-of-the-art is given in Fig. 1.1, where noise temperature for microwave transistors is plotted with respect to frequency. A room temperature bipolar transistor is shown in comparison to room temperature and cryogenic gallium arsenide field effect transistors (GaAs FET's) and high electron mobility transistors (HEMT's). Also included in the figure are sources of external noise in and about the microwave band that

place a fundamental limit on receiver noise temperature. At low frequencies, galactic noise dominates. At high frequencies, the atmospheric absorption effects are evident, due primarily to oxygen and water vapor. In much of the microwave band the only limitation to low noise performance is a small amount of atmospheric absorption and the 3 K cosmic microwave background radiation: a remnant of the intense radiation associated with the *Big Bang*. The cryogenic HEMT stands out as a superior device for low-noise amplification. It provides an alternative to 4 K masers at an enormous reduction in cost [2]. Refrigeration is impractical in most microwave systems, so room temperature HEMT operation near the background radiation limit is the objective of ongoing research.

Recent years have also witnessed dramatic increases in the development and use of microwave computer-aided design (CAD) tools. This has had a profound effect on microwave circuit design strategies. Lab bench tweaking in both the development phase and on the production line have become forbidden in the pursuit of cost effective engineering. Experimentation and development now take place using computer simulations. Efficient algorithms and more accurate component models are continually sought to ensure fast and precise performance prediction. The advent of monolithic microwave integrated circuits has also hastened the development of CAD tools. These allow little on-chip testing and cannot be tweaked or repaired to correct poor performance. Accurate CAD is needed to insure successful first-time chip designs.

While tremendous accomplishments have been made in low-noise transistor technology and microwave CAD development, noise analysis has long been a missing aspect in computer-aided design. When it has been offered, it has typically been restricted to circuits with specific topologies [3], or the effects of correlated noise have been neglected [4]. As a result, the noise performance of many amplifiers could not be accurately predicted prior to fabrication. Only recently have noise analysis methods emerged with the ability to analyze microwave circuits
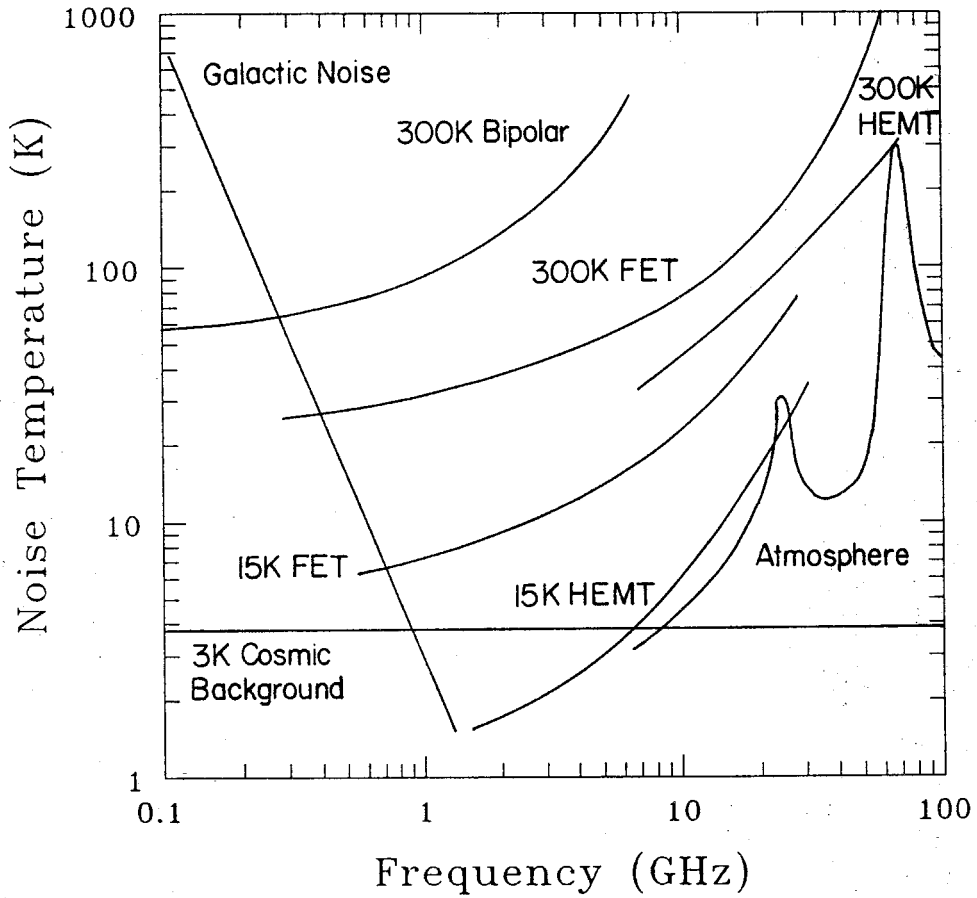
Figure 1.1 Noise temperatures for state-of-the-art microwave transistors compared to natural noise limits.

comprised of arbitrarily interconnected components [5]. Presented here is a new wave variable approach. It is particularly suited to microwave and millimeter-wave circuits which are characterized in terms of wave variables. An integral part of the noise analysis process is the characterization of active microwave devices by both modeling and measurement [6]. New methods to accomplish this using wave variables are also presented. These methods are shown to offer several advantages over current techniques.

1.1 Introduction to Microwave Computer-Aided Design

Predicting the performance of a low noise microwave circuit involves a linear frequency domain analysis. The basic problem is illustrated by Fig. 1.2: given a collection of components, depicted in the figure as S_1, S_2, ..., S_m, the objective is to determine the response of the aggregate network, shown as $\mathbf{S_{net}}$, based on knowledge of the circuit's topology (i.e. the interconnection of the components), and its excitations. The typical computer algorithm obtains a solution by describing the network in terms of Kirchhoff's voltage and current laws and component constitutive relations. This description is used to form one large, although often sparse, matrix equation which when solved gives all values for voltage and current at every node and branch. The large matrix equation is called the *tableau*. Sparse matrix means for its solution are referred to as sparse-tableau methods [7].

A microwave circuit has physical dimensions comparable to a wavelength. Under such conditions voltage and current behave as traveling wave quantities, with impedance mismatches resulting in reflections and standing waves. Voltage and current variations within a circuit can therefore be quite dramatic. Consequently, sparse-tableau methods using voltage and current variables are often numerically unstable. A preferable procedure uses traveling wave variables [8]. In the wave approach, scattering parameters are derived from complex ratios of the wave variables. These parameters form scattering matrices whose manipulation is computationally stable. In the simple example of a one-port element with
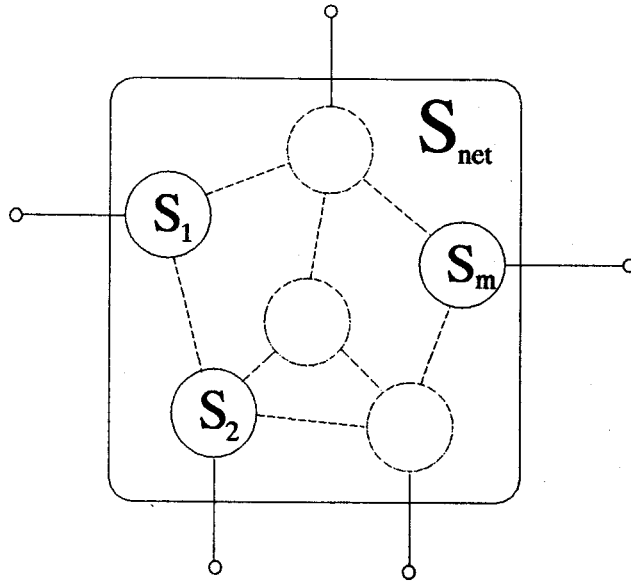
Figure 1.2 A collection of components, S_1, S_2, ..., S_m, interconnected to form network S_{net}. Solid lines depict external connections; dotted lines, internal connections.

impedance $Z(\omega)$ terminating a transmission line with normalizing impedance Z_0, the scattering parameter $S(\omega)$ is given by

$$S(\omega) = \frac{Z(\omega) - Z_o}{Z(\omega) + Z_o}.$$

$$(1.1)$$

If the impedance $Z(\omega)$ is from a passive component, its value will lie in the half-plane given by $Re(Z(\omega)) \geq 0$. The bilinear transform (1.1) maps this half-plane into the unit circle $|S(\omega)| \leq 1$. If $Z(\omega)$ was the impedance of a parallel LC circuit, it would pass through a resonance where $|Z(\omega)|$ tended to infinity. This would result in considerable numerical difficulties if an impedance representation were used. Mapping into the unit circle causes scattering parameters, in comparison, to be well behaved. Since resonances are common in high frequency circuits, the improved numerical stability is welcome.

Scattering matrices have the additional advantage of existing for nearly all networks. Exceptions are caused only by the presence of specific values of negative resistance. In voltage-current methods, nonexistence is a frequent problem and has led to the increased complexity of the modified nodal approach [9]. Simplification is possible using graph theoretic derivation of the tableau [10]. Yet, even simpler graphical methods are possible in the wave approach using Mason's theory of signal-flow graphs [11]. It shall be shown that Mason's theory leads to powerful methods for network reduction and subsequent calculation. These advantages, combined with the fact that scattering parameters are obtained directly during the measurement process, have made the wave approach the preferred method for both microwave component characterization and network analysis [12].

The superiority of the wave approach has led to the hypothesis that a comparable means for performing noise analysis would share its benefits. Noise analysis using wave variables has appeared only recently [13,14]. Much improvement in these methods is possible through application of the *connection theory* presented here. Connection theory has been shown to result in considerable reductions in computer time and memory allocation needs [8]. Historically, it may be traced to Murray-Lasso [15] who conceived the idea of dividing admittance networks into smaller subcircuits to simplify the calculation of the aggregate network. The promise of this idea may be understood by a second look at Fig. 1.2. The connections internal to the network S_{net} are shown with dotted lines. Those connections external to the network, accessible by terminals, are shown in solid lines. Connection theory obtains simplification by avoiding storage and direct calculation of variables associated with the internal connections. Internal and external variables are separated to form a tableau whose solution is derived from a lower order matrix inversion. Such a method using wave variables is given here. It

allows the efficient and simultaneous calculation of both deterministic and noise parameters for interconnected microwave networks of arbitrary topology.

Some of the research described here is based on the author's contributions to the interactive microwave circuit analysis package *PUFF* [16]. Since 1987, this software and accompanying manual have been distributed to over 8000 users in 40 countries. *PUFF* is used to synthesize, analyze, and lay out microstrip and stripline circuits. It is limited, however, to the analysis of deterministic circuits, and cannot perform noise analysis. The features of *PUFF*, plus a noise wave analysis capability, have been combined to form another circuit simulator named *DRACO*. The programs are quite similar, the primary difference being *DRACO*'s ability to perform noise analysis.

1.2 Organization of the Thesis

Given in Fig. 1.3 is a simplified, generic, computer-aided analysis algorithm for the calculation of signal and noise parameters for a network. The two major steps involved are calculation of noise and deterministic parameters for each component, and the application of connection theory to solve for the parameters of the aggregate network. Detailed descriptions of how these steps are accomplished are the subject of this work.

In chapter 2, wave representations for signals and noise are discussed. Defined here is the noise wave correlation matrix used to characterize the statistics of noise sources. Basic manipulations of correlation matrices are described, as well as relationships to two-port figures of merit.

Chapter 3 presents linear connection theory applied to both signal and noise calculations using wave representations. A detailed description of the *subnetwork growth* method is given: the process wherein calculation of a network is made by repeated connection calculations.

Chapter 4 is concerned with the derivation of signal and noise parameters for the basic components used in microwave circuits. These include single and

coupled transmission lines, and microwave transistors. It is shown that in many cases the noise wave parameters can be derived directly from scattering parameters.

The current methods used for the measurement of noise parameters for microwave devices are known to have several limitations [6]. Presented in chapter 5 is an alternative technique used to make direct measurement of noise wave parameters.

Proposed in chapter 6 are research directions in noise analysis and measurement that should be addressed. These areas concern the modeling of microwave devices for noise, and new measurement approaches.
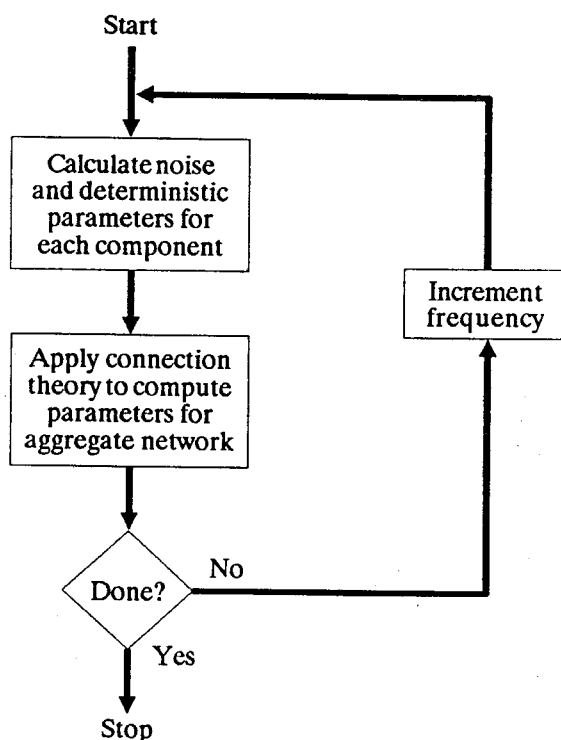

Figure 1.3 Generic computer-aided analysis algorithm for linear frequency domain analysis.

References

[1] S. Vaughn, K. White, U.K. Mishra, M.J. Delaney, P. Greiling, and S. Rosenbaum, "High-performance V-band low noise amplifiers," *IEEE MTT-S Symp. Dig.*, pp. 801-804, 1989.

[2] M.W. Pospieszalski, S. Weinreb, R.D. Norrod, and R. Harris, "FET's and HEMT's at cryogenic temperatures – their properties and use in low-noise amplifiers," *IEEE Trans. Microwave Theory Tech.*, vol. MTT-36, pp. 552-560, Mar. 1988.

[3] H. Hillbrand and P.H. Russer, "An efficient method for computer aided noise analysis of linear amplifier networks," *IEEE Trans. Circuits Syst.*, vol. CAS-23, pp. 235-238, April 1976.

[4] R. Rohrer, L. Nagel, R. Meyer, and L. Weber, "Computationally efficient electronic–circuit noise calculations," *IEEE J. Solid-State Circuits*, vol. SC-6, pp. 204-213, Aug. 1971.

[5] V. Rizzoli and A. Lipparini, "Computer–aided noise analysis of linear multiport networks of arbitrary topology," *IEEE Trans. Microwave Theory Tech.*, vol. MTT-33, pp. 1507-1512, Dec. 1985.

[6] A. Cappy, "Noise modeling and measurement techniques," *IEEE Trans. Microwave Theory Tech.*, vol. MTT-36, pp. 1-10, Jan. 1988.

[7] G. D. Hachtel, R. K. Brayton, and F. G. Gustavson, "The sparse tableau approach to network analysis and design," *IEEE Trans. Circuit Theory*, vol. CT-18, pp. 101-113, Jan. 1971.

[8] V. A. Monaco and P. Tiberio, "Computer-aided analysis of microwave circuits," *IEEE Trans. Microwave Theory Tech.*, vol. MTT-22, pp. 249-263, Mar. 1974.

[9] C. Ho, A.E. Ruehli, and P.A. Brennan, "The modified nodal approach to network analysis," *IEEE Trans. Circuits Syst.*, vol. CAS–25, pp. 504-509, June 1975.

[10] J. Vlach and K. Singhal, *Computer Methods for Circuit Analysis and Design*, Van Nostrand Reinhold, New York, 1983.

[11] S.J. Mason, "Feedback theory – further properties of signal flow graphs," *Proc. IRE*, vol. 44, pp. 920–926, July 1956.

[12] K.C. Gupta, R. Garg, and R. Chadha, *Computer–Aided Design of Microwave Circuits*, Artech House, Norwood, Massachusetts, 1981.

[13] N.G. Kanaglekar, R.E. McIntosh, and W.E. Bryant, "Wave analysis of noise in interconnected multiport networks," *IEEE Trans. Microwave Theory Tech.*, vol. MTT-35, pp. 112–115, Feb. 1987.

[14] J.A. Dobrowolski, "A CAD–oriented method for noise figure computation of two-ports with any internal topology," *IEEE Trans. Microwave Theory Tech.*, vol. MTT-37, pp. 15–20, Jan. 1989.

[15] M.A. Murray-Lasso, "Black-box models for linear integrated circuits," *IEEE Trans. Educ.*, vol. E-12, pp. 170-180, Sept. 1969.

[16] R. Compton, S.W. Wedge, and D. Rutledge, *PUFF: Computer-Aided Design for Microwave Integrated Circuits*, published at Caltech, Pasadena, California, Jan. 1990.

Chapter 2

Representation of Noisy Circuits

A large body of work has been devoted to noise representations for two-port circuits. Hartmann [1] surveys twelve different methods, showing that each requires four noise and four complex signal parameters per frequency. The use of multiple representations is common because each offers a simple noise calculation for components connected in a specific manner. The computer-aided noise analysis strategy has been to use the appropriate noise representation for the type of connection to be made [2]. The advantages are akin to deterministic methods: admittance matrices allow a simple calculation for parallel circuits, impedance matrices simplify the series connection, and the chain representation simplifies the cascade connection. This approach works well for interconnected two-ports. For arbitrarily interconnected multiports, however, the types of connections and hence the number of definable representations are essentially unlimited.

For the analysis of arbitrarily complex circuits, the representation must be applicable to any number of ports. The chain representation, for example, uses both noise voltage and current sources and has a multiport equivalent only when an even number of ports is considered [3]. The deterministic and noise properties of a circuit must be characterized in a compatible manner. Noise modeling with an admittance matrix, for example, requires noise current sources, while noise voltage sources would be used with an impedance matrix. As discussed in chapter 1, these representations use ratios of voltage and current that can be

numerically unstable in microwave circuits. Scattering matrices are considered superior. In contrast to the traditional use of noise voltage and current sources, a representation compatible with scattering parameters shall be developed here using noise wave sources. Wave representations for noise are not new. Bauer and Rothe [4] and Penfield [5] gave examples soon after Rothe and Dahlke published their definitive theory of noisy fourpoles [6] using correlated voltage and current sources. Bosma [7], using a noise wave approach, has reworked the Haus and Adler [3] optimum noise performance problem. The noise wave definitions given here are similar to those used by Bosma. They allow generalized analysis methods, and parameterization based on statistical properties.

2.1 Scattering Parameters and Traveling Noise Waves

Given in Fig. 2.1 is a transmission line of characteristic impedance Z_0 terminated in an impedance $Z(\omega)$. A deterministic voltage wave V_+, traveling in the positive z direction, is incident from the left. It is scattered, resulting in the voltage wave V_- traveling in the opposite direction. In phasor notation, the deterministic voltage waves V_+ and V_- have the form

$$V_+ = A e^{j\phi_+} e^{-j\beta z} \qquad (2.1a)$$

$$V_- = B e^{j\phi_-} e^{j\beta z} \qquad (2.1b)$$

where A and B are rms magnitudes, β is the propagation constant, and ϕ_+ and ϕ_- are phases. The scattering parameter representation is made in reference to normalized values of these voltage waves, given by

$$a = \frac{V_+}{\sqrt{Z_0}} \qquad b = \frac{V_-}{\sqrt{Z_0}} \qquad (2.2)$$

where Z_0 is the real characteristic or normalizing impedance of the line, a is the incident wave, and b the scattered wave. This normalization results in the power propagating in the positive and negative z direction to be given by $|a|^2$ and $|b|^2$,

respectively. The scattering parameter S is the ratio of the two traveling waves, and the one-port circuit of Fig 2.1 is represented by the simple expression

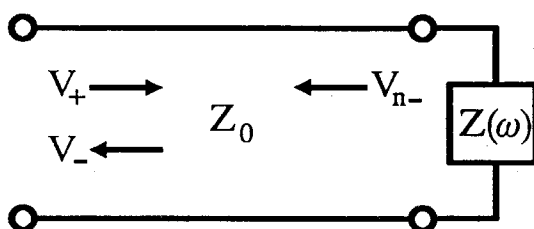$$b = Sa \tag{2.3}$$

where S may be found from (1.1).

Figure 2.1 A transmission line with characteristic impedance Z_0 terminated in an impedance $Z(\omega)$. Voltage wave V_+ is incident, causing scattering wave V_-. Wave V_{n-} is due to noise.

The above result does not account for noise that could be produced by the terminating impedance. For example, a passive $Z(\omega)$ would produce an output wave due to its thermal noise. This wave will be a random variable, but if confined to a small bandwidth Δf about a mean frequency $\overline{f}$, it may be written with a phasor defined at $\overline{\omega} = 2\pi\overline{f}$ in a manner similar to the deterministic waves, namely

$$V_{n-}(t) = C(t)e^{j\phi_n(t)}e^{j\overline{\beta}z} \tag{2.4}$$

where $\overline{\beta}$ is the mean propagation constant at $\overline{f}$. Random variables $C(t)$ and $\phi_n(t)$ describe the rms amplitude and phase, respectively, of the wave envelope. Assuming $\Delta f \ll \overline{f}$, these will be slowly varying functions. This leads to the definition of a normalized noise wave c given by

$$c = c(t) = \frac{V_{n-}(t)}{\sqrt{Z_0}}. \tag{2.5}$$

Since $V_{n-}(t)$ is given in terms of an rms phasor, $|c|^2$ will have units of power, as in the case of $|a|^2$ and $|b|^2$. Although c is a time varying complex random variable, its randomness and time dependence are removed by its characterization in terms of time averaged power $\overline{|c|^2}$ given by [8]

$$\overline{|c|^2} = \lim_{T \to \infty} \frac{1}{2T} \int_{-T}^{+T} |c(t)|^2 dt. \tag{2.6}$$

In general, the value of $\overline{|c|^2}$ will be a function of both $\overline{f}$ and Δf.

Based on these definitions, it is now possible to rewrite (2.3) to include the effects of the one-port termination's noise. This is done by adding a wave source term c:

$$b = Sa + c. \tag{2.7}$$

The output wave b now includes contributions from both the scattered wave Sa, and the noise wave. A complete representation for the one-port now includes the scattering parameter S and the noise power $\overline{|c|^2}$ that is available from the termination.

The result of (2.7) can be generalized to the case of an arbitrary multiport network. Given in Fig. 2.2 is a multiport network **S** with incident waves $a_1, a_2, \ldots, a_n$ and output waves $b_1, b_2, \ldots, b_n$ present at each terminal. As in the case of the one port, these are normalized traveling waves defined as in (2.2). Elements of the scattering matrix, or S-matrix, are defined in terms of complex ratios of these waves

$$s_{ij} = \frac{b_i}{a_j} \bigg|_{\substack{a_k = 0 \\ \forall k \neq j}} \tag{2.8}$$

where noise sources are neglected and the restriction that a_j is the only incident wave implies that all other ports are terminated in the normalizing impedance Z_0. The diagonal elements, s_{ii}, of the S-matrix thus represent reflection coefficients, while the off-diagonal elements, s_{ij}, represent either gain or isolation.
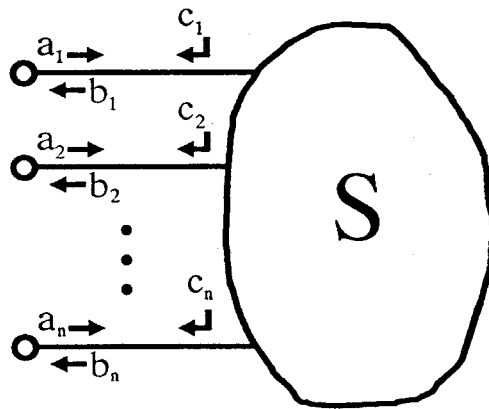
Figure 2.2 A multiport network S with incident waves $a_1, a_2, \ldots, a_n$, output waves $b_1, b_2, \ldots, b_n$, and noise waves $c_1, c_2, \ldots, c_n$, present at each port.

To model the effects of noise, Fig. 2.2 includes wave sources $c_1, c_2, \ldots, c_n$ that represent contributions to the output waves due to the multiport's internal noise. These noise waves are outwardly directed correlated sources present at each port, defined as in (2.5), and represent the noise originating in the network that is deliverable to its terminations. For the general multiport element, the relation between incident and output waves is therefore given by the matrix equation

$$\mathbf{b} = \mathbf{Sa} + \mathbf{c} \qquad (2.9)$$

where **a** and **b** are vectors denoting incident and output waves, respectively, **S** is the scattering matrix, and the noise waves are given by vector **c**. A physical interpretation of the noise waves is in order. Based on the definition of (2.9) they may be found mathematically by satisfying

$$\mathbf{c} = \mathbf{b} \Big|_{\mathbf{a}=\mathbf{0}} . \qquad (2.10)$$

It is therefore tempting to define **c** as those waves the network **S** delivers into non-reflective terminations in the absence of input. Yet, physically such an absence is

unrealizable: the multiport would have to be terminated in non-reflective loads (i.e. characteristic impedances Z_0) that produce no noise, implying resistive terminations at 0 K. Noise emanating from the terminations will always yield a nonzero **a** vector which in general will be scattered by **S** and contribute to **b**. The noise wave vector **c** is therefore best interpreted as the *excess* noise wave that the multiport delivers to its terminations.

2.2 The Noise Wave Correlation Matrix

As in the case of the one-port, the components of **c** are complex random variables. Parameterization is required in terms of their statistical properties. This is accomplished through definition of the noise wave correlation matrix $\mathbf{C_s}$ given by

$$\mathbf{C_s} = \overline{\mathbf{cc^\dagger}} \tag{2.11}$$

where the dagger indicates Hermitian conjugation, and the overbar indicates statistical averaging. The components of the matrix are the correlation products $\overline{c_i c_j^*}$

$$\overline{c_i c_j^*} = \lim_{T \to \infty} \frac{1}{2T} \int_{-T}^{+T} c_i(t) c_j^*(t) dt \tag{2.12}$$

where, as before, $\overline{c_i c_j^*}$ is in general a function of both $\overline{f}$ and Δf. For the arbitrary multiport of Fig. 2.2, the noise wave correlation matrix is written

$$\mathbf{C_s} = \begin{pmatrix} \overline{|c_1|^2} & \overline{c_1 c_2^*} & \cdots & \overline{c_1 c_n^*} \\ \overline{c_2 c_1^*} & \overline{|c_2|^2} & \cdots & \overline{c_2 c_n^*} \\ \vdots & \vdots & \ddots & \vdots \\ \overline{c_n c_1^*} & \overline{c_n c_2^*} & \cdots & \overline{|c_n|^2} \end{pmatrix}. \tag{2.13}$$

For each noise-wave c_i the correlation matrix yields values for the noise power deliverable to the terminations, given by $\overline{|c_i|^2}$, as well as a correlation product with each of the other ports, given by $\overline{c_i c_j^*}$. An n-port linear component's signal and noise properties are completely described by $n \times n$ scattering and noise wave correlation matrices.

Specific conditions must be met in order for the noise wave correlation matrix to exist. Noise waves are defined in a bandwidth Δf about a mean frequency $\bar{f}$, so a frequency domain representation of the statistics of the waves must be possible. This is guaranteed by considering only noise processes that are wide-sense stationary. When more than one process is considered (i.e. cross-correlation between noise waves) these must be jointly wide-sense stationary. The processes must also be ergodic to ensure that the time limits given in (2.6) and (2.12) exist and correspond to ensemble averages. When two noise processes c_i and c_j meet these conditions, the correlation product $\overline{c_i c_j^*}$ can be represented approximately by

$$\overline{c_i c_j^*} \approx 2\Delta f W_{ij}(\bar{f}) \qquad (2.14)$$

where W_{ij} is the self ($i = j$) or cross ($i \neq j$) power spectral density of the two processes, assumed to have little variation over the bandwidth Δf. The factor of two accounts for the two-sidedness of the spectral density function. The approximation may be made arbitrarily close by letting Δf approach zero. For the purpose of numerical manipulation the Δf is often dropped. An assumption is made either that $\Delta f = 1$ Hz or that the correlation terms are power density. A power density interpretation changes approximation (2.14) to an exact relation. In either case, the values of the correlation matrix are referred to as *spot noise* values.

Values of Δf can be significant when related to measurement of the noise waves. Coherence length and time will be set by the measurement system. A system with group velocity v_g will have a coherence length given by $\Delta \ell = v_g / \Delta f$ and coherence time $\Delta t = 1/\Delta f$. The dimensions and bandwidth of the measurement system must be such that the random variables of (2.4) are sufficiently slowly varying to allow noise wave comparisons. A transmission line system will typically have multiple reflections that must be taken into account. Requiring

phase changes due to coherence length and time to be much less than 2π results in the criteria

$$nL \ll \Delta\ell \tag{2.15}$$

where n is an integer accounting for the number of reflections, and L is the physical dimension of the measurement system that accounts for wave delays. A typical spectral density measurement of a microwave circuit will have $\Delta f \approx 4$ MHz, and easily satisfy (2.15). This is often combined with a long integration time to improve the estimation of (2.12).

2.3 Transformations

A noise wave correlation matrix will undergo a transformation upon operation by a linear system. For example, a noise wave vector $\mathbf{c}$, may be modified by a transformation $\mathbf{T}$ resulting in a vector $\mathbf{c}' = \mathbf{Tc}$. The original noise wave correlation matrix $\mathbf{C_s} = \overline{\mathbf{cc}^\dagger}$ will therefore undergo an Hermitian congruence transformation to a new matrix given by

$$\mathbf{C_s}' = \mathbf{TC_sT}^\dagger \tag{2.16}$$

The general form of (2.16) is apparent in any transformation of a correlation matrix. Such transformations occur when components are added to a network, and shall be considered in detail in the next chapter.

Changing from one noise representation to another is the equivalent of operation by a linear system. Such a change may be made for computational advantage or to avoid singularities. In addition to the wave approach, admittance and impedance representations have applications. All three are compared in Fig. 2.3 including their respective circuit diagrams and matrix relations for voltage, current, and wave quantities. Methods using impedance matrices and noise voltage sources have been described by Haus and Adler [9], while noise

analysis using admittance matrices and noise current sources has been discussed by Rizzoli and Lipparini [10]. The correlation matrices are defined similarly

$$\mathbf{C_y} = \overline{\mathbf{i_n i_n^\dagger}} \tag{2.17a}$$

$$\mathbf{C_s} = \overline{\mathbf{v_n v_n^\dagger}} \tag{2.17b}$$

where $\mathbf{i_n}$ is the noise current vector of the admittance representation and $\mathbf{v_n}$ is the noise voltage vector of the impedance representation.

Relations between wave, voltage and current quantities for both signals and noise are necessary to derive transformations. The signal traveling waves used to define the scattering matrix are related to the terminal voltage and current of the multiport by

$$\mathbf{a} = \tfrac{1}{2}(\mathbf{v} + \mathbf{i}) \tag{2.18a}$$

$$\mathbf{b} = \tfrac{1}{2}(\mathbf{v} - \mathbf{i}) \tag{2.18b}$$

where normalization to the characteristic impedance has been assumed. These identities allow derivation of the signal matrix transformations given in Fig. 2.3.

Comparison of noise quantities is assisted by defining the following waves in terms of the multiport's short circuit noise current and open circuit noise voltage

$$\mathbf{a_n} = \tfrac{1}{4}(\mathbf{v_n} + \mathbf{i_n}) \tag{2.19a}$$

$$\mathbf{b_n} = \tfrac{1}{4}(\mathbf{v_n} - \mathbf{i_n}) \tag{2.19b}$$

where again normalization to the characteristic impedance is assumed. The noise wave vector is then given by

$$\mathbf{c} = \mathbf{b_n} - \mathbf{S a_n} \tag{2.20}$$

where $\mathbf{S}$ is the scattering matrix. Relations (2.19)-(2.20) lead to the family of noise correlation matrix transformations, also listed in Fig. 2.3.
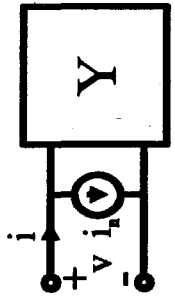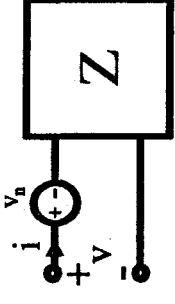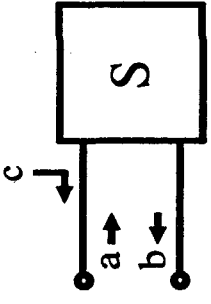
Representation	Admittance	Impedance	Wave
Circuit Diagram			
General Identities	$i = Yv + i_n$ $C_y = \overline{i_n i_n^\dagger}$	$v = Zi + v_n$ $C_z = \overline{v_n v_n^\dagger}$	$b = Sa + c$ $C_s = \overline{cc^\dagger}$
Signal Matrix Transformations	$Y = Z^{-1}$ $Y = (I - S)(I + S)^{-1}$	$Z = Y^{-1}$ $Z = (I + S)(I - S)^{-1}$	$S = (Z + I)^{-1}(Z - I)$ $S = (I + Y)^{-1}(I - Y)$
Correlation Matrix Transformations	$C_y = YC_z Y^\dagger$ $C_y = (I + Y)C_s(I + Y)^\dagger$	$C_z = ZC_y Z^\dagger$ $C_z = (I + Z)C_s(I + Z)^\dagger$	$C_s = \frac{1}{4}(I + S)C_y(I + S)^\dagger$ $C_s = \frac{1}{4}(I - S)C_z(I - S)^\dagger$

Figure 2.3 Comparison of admittance, impedance, and wave parameters.

2.4 Indefinite Multiport Representations

Signal matrix and noise correlation matrix data derived from swept frequency measurements are often used in the computer-aided design process. Often these data are unsuitable for direct numerical manipulation. Active devices are generally measured with one terminal grounded, and the resulting *definite* parameters, so named because a clearly defined ground connection exists, characterize the N terminal device in terms of an $N - 1$ multiport. In the case of transistors, two-port common source or common emitter measurements characterize the three terminal device. These definite parameters must be converted to a form that allows the device to be placed in any configuration, and not simply the common source or common emitter configuration in which it was measured. *Indefinite* parameters provide the solution. The indefinite parameters of an N terminal device may be derived from its definite parameters by mathematically changing the grounded terminal into an accessible terminal. This yields the desired N-port characterization of the N terminal device.

An indefinite multiport is defined as one in which no internal connection to ground exists. The terminal currents then satisfy Kirchhoff's current law (KCL)

$$\sum_{j=1}^{N} i_j = 0. \tag{2.21}$$

At microwave frequencies this condition is not assured. Currents to ground resulting from stray capacitance would not pass through a terminal, and would result in errors. When KCL is valid, the use of an impedance representation is precluded; indefinite impedance matrices do not exist. In terms of admittance and scattering parameters, KCL results in useful properties. For an indefinite admittance matrix, (2.21) causes the sum of any row or column in the matrix to equal zero, the components satisfying

$$\sum_{j=1}^{N} y_{jk} = \sum_{k=1}^{N} y_{jk} = 0. \tag{2.22}$$

This result facilitates the conversion from definite to indefinite parameters. Connecting a terminal of a multiport admittance to ground will reduce its matrix by one row and one column, but will not affect the remaining components. The definite and indefinite matrix components y_{jk} will be identical for $j, k < N$. The definite parameters fill most of the indefinite matrix; only a single row and column need be generated, and this is possible using (2.22).

In the case of scattering parameters, the enforcement of KCL results in the sum of any row or column in the indefinite scattering matrix to equal unity; the components satisfying

$$\sum_{j=1}^{N} s_{jk} = \sum_{k=1}^{N} s_{jk} = 1. \tag{2.23}$$

Since definite and indefinite scattering matrices generally do not share common components, (2.23) does not allow a simple conversion between the two. Instead it permits $N - 1$ port scattering parameter measurements to be used to fill an N port indefinite matrix if the N'th port of the device is terminated in the normalizing impedance during measurement [11]. Parameters can then be shared, and the N'th row and column of the indefinite matrix would be filled using (2.23). When measurements are performed with the N'th terminal connected to ground, however, the conversion to an indefinite scattering matrix is best made using transformations to and from the admittance representation given in Fig. 2.3.

Multiport noise correlation matrices may also be converted from definite to indefinite forms. Based on the general identities given in Fig. 2.3, the noise currents in an indefinite multiport admittance must also satisfy KCL. It then follows that the sum of any row or column in an indefinite noise current correlation matrix $\mathbf{C_y}$ is equal to zero:

$$\sum_{j=1}^{N} \overline{i_{nj} i_{nk}^*} = \sum_{k=1}^{N} \overline{i_{nj} i_{nk}^*} = 0. \tag{2.24}$$

As in the case of the deterministic admittance matrix (for $j, k < N$) the values $\overline{i_{nj} i_{nk}^*}$ are the same for definite and indefinite matrices. The indefinite noise current correlation matrix is therefore easily filled using (2.24) and the values from the definite matrix.

In the case of the indefinite noise wave correlation matrix, KCL and the relations in Fig. 2.3 lead to the result that

$$\sum_{j=1}^{N} \overline{c_j c_k^*} = \sum_{k=1}^{N} \overline{c_j c_k^*} = 0. \tag{2.25}$$

The sum of any row or column in $\mathbf{C_s}$ equals zero, as well. As with scattering parameters, conversion from a definite to an indefinite noise wave correlation matrix is difficult since they do not share common components. As before, however, if $N-1$ port noise measurements are performed with the N'th port terminated in the appropriate normalizing impedance, these measurements and (2.25) can be used to fill the indefinite matrix. When the noise measurements are performed with the N'th terminal grounded, the generation of the indefinite noise wave matrix is best made using the transformations given in Fig. 2.3.

2.5 Analysis of Noisy Two-Ports

Although a microwave circuit may consist of a complicated arrangement of various components, the result is often a two-port device. A noise performance appraisal for the two-port is made using well known figures of merit. These may be calculated using values of the scattering and noise wave correlation matrices.

Noise figure (F) has been defined by Friis [12] as a measure of the degradation in signal-to-noise ratio. It may be written as

$$F = 1 + \frac{N_a}{G_a N_s} \tag{2.26}$$

where N_a is the noise power added by the two-port that is available at its output, G_a is the available power gain, and N_s is the thermal noise power available from a

source assumed to be at temperature $T_0 = 290\ K$. This definition can be applied to the two-port amplifier represented by scattering parameters and noise waves as given in Fig. 2.4(a). An input signal source is shown as reflection coefficient Γ_s. The two-port has outward directed noise waves c_1 and c_2. The noise waves are shown as source terms in the signal-flow graph of Fig. 2.4(b) [13]. The nodes on the graph denote traveling wave variables while the branches represent transfer (i.e. scattering) coefficients. Mason's theory [14] is used to solve for the needed quantities. The available gain of the two-port is

$$G_a = \frac{|s_{21}|^2 (1 - |\Gamma_s|^2)}{|1 - \Gamma_s s_{11}|^2 (1 - |s'_{22}|^2)} \tag{2.27}$$

where s'_{22} is the equivalent reflection coefficient seen at the output of the two-port given by

$$s'_{22} = s_{22} + \frac{s_{12}\Gamma_s s_{21}}{1 - \Gamma_s s_{11}}. \tag{2.28}$$

The thermal noise power available from the source is known from Nyquist's formula to be

$$N_s = kT_0 \tag{2.29}$$

where k is Boltzmann's constant and a 1-Hz bandwidth is assumed. The available noise power added by the two-port is also found by evaluation of the signal-flow graph. The noise power at the output is found by adding contributions to node b_2 due to c_1 and c_2. This gives
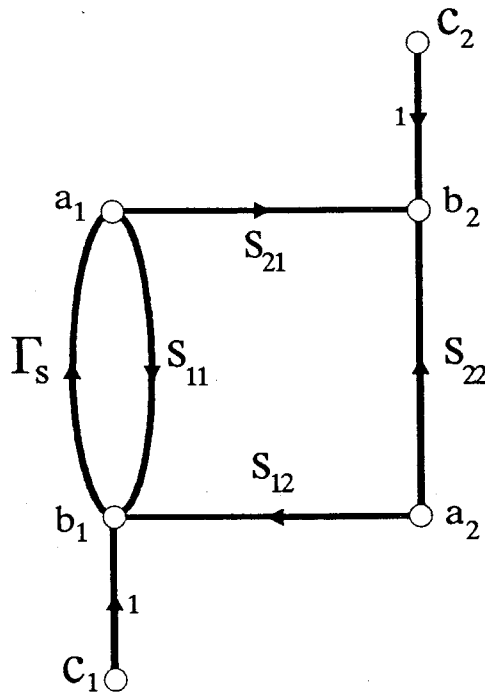
$$N_a = \frac{\overline{\left| c_1 \left(\dfrac{\Gamma_s s_{21}}{1 - \Gamma_s s_{11}} \right) + c_2 \right|^2}}{1 - |s'_{22}|^2}. \tag{2.30}$$

Substitution of the above expressions into (2.26) results in

$$F = 1 + \frac{\overline{\left| c_1 \Gamma_s + c_2 \left(\dfrac{1 - \Gamma_s s_{11}}{s_{21}} \right) \right|^2}}{kT_0 (1 - |\Gamma_s|^2)}. \tag{2.31}$$
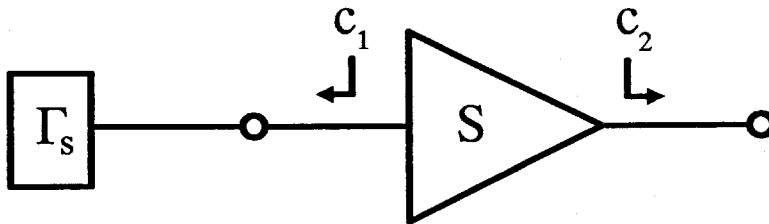
(a)

(b)

Figure 2.4 Schematic (a) and signal-flow graph (b) diagrams for a noisy two-port component.

The numerator can be expanded and written in terms of the two-port's noise wave correlation matrix $\mathbf{C_s}$. Doing so and writing the result in terms of noise temperature $T_n = T_0(F - 1)$ gives

$$kT_n = \frac{\beta \mathbf{C_s} \beta^\dagger}{(1 - |\Gamma_s|^2)} \tag{2.32}$$

where β is the 1×2 row matrix given by

$$\beta = \left(\Gamma_s \quad \frac{1 - \Gamma_s s_{11}}{s_{21}} \right). \tag{2.33}$$

Haus and Adler [3] have defined the figure of merit known as noise measure which determines the best cascade order of two amplifiers with respect to the noise performance. It takes into account the amplifier gain that, if small, would cause poor cascaded noise figure. Applying the definition given by Fukui [15] gives

$$M = \frac{F - 1}{1 - \dfrac{1}{G_a}} = -\frac{\beta \mathbf{C_s} \beta^\dagger}{kT_0 \beta(\mathbf{I} - \mathbf{SS^\dagger})\beta^\dagger} \tag{2.34}$$

where $\mathbf{S}$ is the scattering matrix of the two-port, and again a 1-Hz bandwidth has been assumed.

Equations (2.32) and (2.34) demonstrate that if the noise correlation matrix of the two-port is known, then its noise figure, noise temperature, and noise measure can be predicted as a function of the source reflection coefficient. It is not typical, however, to make direct measurement of the components of $\mathbf{C_s}$. Instead, two-port measurements are commonly made to extract the noise parameters known as T_{min} (minimum noise temperature), Γ_{opt} (optimum source reflection coefficient), and R_n (noise resistance). These parameters satisfy the noise temperature relation

$$T_n = T_{min} + \frac{4 T_0 R_n}{Z_0} \frac{|\Gamma_s - \Gamma_{opt}|^2}{|1 + \Gamma_{opt}|^2 (1 - |\Gamma_s|^2)}. \tag{2.35}$$

By comparing (2.35) and (2.32), conversion formulas between the above noise parameters and elements of the noise wave correlation matrix may be derived. These are

$$\overline{|c_1|^2} = kT_{min}\left(|s_{11}|^2 - 1\right) + \frac{kt|1 - s_{11}\,\Gamma_{opt}|^2}{|1 + \Gamma_{opt}|^2} \tag{2.36a}$$

$$\overline{|c_2|^2} = |s_{21}|^2\left(kT_{min} + \frac{kt|\Gamma_{opt}|^2}{|1 + \Gamma_{opt}|^2}\right) \tag{2.36b}$$

$$\overline{c_1 c_2^*} = \frac{-s_{21}^*\Gamma_{opt}^*\,kt}{|1 + \Gamma_{opt}|^2} + s_{11}\,s_{21}^*\left(\frac{kt|\Gamma_{opt}|^2}{|1 + \Gamma_{opt}|^2} + kT_{min}\right) \tag{2.36c}$$

where

$$kt = \frac{4\,kT_0R_n}{Z_0}. \tag{2.37}$$

The inverse relations are

$$kt = \overline{\left|c_1 - c_2\left(\frac{1 + s_{11}}{s_{21}}\right)\right|^2} \tag{2.38a}$$

$$kT_{min} = \frac{\overline{|c_2|^2} - \overline{|c_1 s_{21} - c_2 s_{11}|^2}|\Gamma_{opt}|^2}{|s_{21}|^2(1 + |\Gamma_{opt}|^2)} \tag{2.38b}$$

$$\Gamma_{opt} = \frac{\eta}{2}\left(1 - \sqrt{1 - \frac{4}{|\eta|^2}}\right) \tag{2.38c}$$

where

$$\eta = \frac{\overline{|c_2|^2} + \overline{|c_1 s_{21} - c_2 s_{11}|^2}}{\overline{|c_2|^2}s_{11} - \overline{c_1 c_2^*}s_{21}}. \tag{2.39}$$

These relations are rather complicated, but some insight can be gained by defining the denominator of η as a parameter ζ given by

$$\zeta = \overline{|c_2|^2}s_{11} - \overline{c_1 c_2^*}s_{21}. \tag{2.40}$$

This parameter represents a measure of the correlation between c_1 and c_2 referenced at an input node. The following relations exist between Γ_{opt} and ζ:

$$\lim_{|\zeta| \to 0} |\Gamma_{opt}| = 0 \qquad (2.41a)$$

$$\arg(\Gamma_{opt}) = -\arg(\zeta) \qquad (2.41b)$$

i.e., when the correlation term ζ vanishes, T_{min} has been obtained, and a $180°$ phase difference exists between ζ and Γ_{opt}. The search for an optimum noise match using the noise wave correlation matrix thus involves finding a network that gives $\zeta = 0$. Since impedance matching is also of concern, this can be interpreted as a search to make $\overline{c_1 c_2^*} = 0$ and $s_{11} = 0$.

The complexity of the conversion formulas given above is due to differences in the nature of the noise parameter definitions, each being a function of Γ_s. As apparent in (2.35), the noise parameters Γ_{opt}, T_{min}, and R_n are defined in such a way as to lead to a simple expression for T_n when $\Gamma_s = \Gamma_{opt}$. The noise wave correlation matrix parameters, however, lead to a simple expression for $\Gamma_s = 0$. Substitution of $\Gamma_s = 0$ into (2.32) and (2.34) results in

$$kT_n = \frac{\overline{|c_2|^2}}{|s_{21}|^2} \qquad (2.42)$$

for noise temperature and

$$M = \frac{\overline{|c_2|^2}}{|s_{21}|^2 + |s_{22}|^2 - 1} \qquad (2.43)$$

for noise measure. The single output noise power $\overline{|c_2|^2}$ of the two-port is the sole indicator of noise performance with a non-reflective (Z_0) input termination.

Using noise parameters referenced to Z_0 terminations permits a new low noise design process. The traditional procedure is to create a matching network that transforms a $\Gamma_s = 0$ load to $\Gamma_s = \Gamma_{opt}$. This network is then connected to the input of the device to realize T_{min}. This is an inside-out approach: the

matching network and the device to be matched have been divided and analyzed separately. Noise waves permit an outside-in approach. The complete circuit, including matching network and device, is built up and analyzed as a whole. Each change will, in general, cause a change in the correlation matrix, and lead to new values for T_n (2.42). The T_{min} design is known to be realized when $\zeta = 0$, or alternatively, when $\overline{c_1 c_2^*}$ and s_{11} are nulled. The approach is compatible with deterministic amplifier design using scattering parameters, where a typical objective is to null s_{11} and s_{22} for good input and output matching. In chapter 5, methods shall be shown for the direct measurement of noise waves in a Z_0 system. In general, the outside-in approach has the advantage that the parameters calculated are also those that are measured.

References

[1] K. Hartmann, "Noise characterization of linear circuits," *IEEE Trans. Circuit Syst.*, vol. CAS-23, pp. 581-590, Oct. 1976.

[2] H. Hillbrand and P.H. Russer, "An efficient method for computer aided noise analysis of linear amplifier networks," *IEEE Trans. Circuits and Systems*, vol. CAS-23, pp. 235-238, April 1976.

[3] H.A. Haus and R.B. Adler, "Optimum noise performance of linear amplifiers," *Proc. IRE*, vol. 46, pp. 1517-1533, Aug. 1958.

[4] H. Bauer and H. Rothe, "Der äquivalente Rauschvierpol als Wellenvierpol," *Arch. elekt. Übertragung*, vol. 10, pp. 241-252, June 1956.

[5] P. Penfield, "Wave representation of amplifier noise," *IRE Trans. Circuit Theory*, vol. CT-9, pp. 84-86, Mar. 1962.

[6] H. Rothe and W. Dahlke, "Theory of noisy fourpoles," *Proc. IRE*, vol. 44, pp. 811-818, June 1956.

[7] H. Bosma, "On the theory of linear noisy systems," *Phillips Res. Repts. Suppl.*, no. 10, 1967.

[8] W.B. Davenport and W.L. Root, *An Introduction to the Theory of Random Signals and Noise*, McGraw Hill, New York, 1958.

[9] H.A. Haus and R.B. Adler, *Circuit Theory of Linear Noisy Networks*, John Wiley & Sons, New York, 1959.

[10] V. Rizzoli and A. Lipparini, "Computer-aided noise analysis of linear multiport networks of arbitrary topology," *IEEE Trans. Microwave Theory Tech.*, vol. MTT-33, pp. 1507-1512, Dec. 1985.

[11] A.P. Anderson, "High-frequency transistor evaluation by three-port scattering parameters," *IEEE Trans. Microwave Theory Tech.*, vol. MTT-15, pp. 263-265, April 1967.

[12] H.T. Friis, "Noise figures of radio receivers," *Proc. IRE*, vol. 32, pp. 419-422, July 1944.

[13] R.P. Hecken, "Analysis of linear noisy two-ports using scattering waves," *IEEE Trans. on Microwave Theory and Tech.*, vol. MTT-29, pp. 997-1004, Oct. 1981.

[14] S.J. Mason, "Feedback theory – further properties of signal flow graphs," *Proc. IRE*, vol. 44, pp. 920-926, July 1956.

[15] H. Fukui, "Available power gain, noise figure, and noise measure of two-ports and their graphical representation," *IEEE Trans. Circuit Theory*, vol. CT-13, pp. 137-142, June 1966.

Chapter 3

Linear Connection Theory

In the wave approach to network analysis, direct application of Kirchhoff's laws is inappropriate. Alternatives are sought that allow sufficient mathematical circuit descriptions to permit network solution. These come in two forms: wave equivalence based on network connections, and signal-flow graph theory. Combined, these form the basis of linear connection theory.

As with any approach, a network is solved based on knowledge of its components and its topology. Both brute force and elegant means of solution are typically possible. For the computer, the brute force method involves placing all network information in a large matrix called the tableau. Solution is then accomplished by matrix inversion. In this chapter, the brute force method shall first be examined. This is followed by pursuit of more elegant means to simplify the matrix inversion problem to reduce computer time and memory space requirements. This leads to the subnetwork growth method: a numerical application of signal-flow graph theory.

3.1 Multiport Wave Variable Connection Methods

The basic network analysis problem is illustrated by Fig. 3.1(a). A group of components S_1, S_2, ..., S_m, have been combined to form network $\mathbf{S_{net}}$. In the wave variable interpretation, these components are represented by scattering matrices. Associated with each multiport scattering matrix $\mathbf{S_k}$ shall be an input wave vector $\mathbf{a_k}$, an output wave vector $\mathbf{b_k}$, and an output wave source vector $\mathbf{c_k}$. All of these variables may be placed into a tableau equation given by

$$\begin{pmatrix} \mathbf{b_1} \\ \mathbf{b_2} \\ \vdots \\ \mathbf{b_m} \end{pmatrix} = \begin{pmatrix} \mathbf{S_1} & \mathbf{0} & \dots & \mathbf{0} \\ \mathbf{0} & \mathbf{S_2} & \dots & \mathbf{0} \\ \vdots & \vdots & \ddots & \vdots \\ \mathbf{0} & \mathbf{0} & \dots & \mathbf{S_m} \end{pmatrix} \begin{pmatrix} \mathbf{a_1} \\ \mathbf{a_2} \\ \vdots \\ \mathbf{a_m} \end{pmatrix} + \begin{pmatrix} \mathbf{c_1} \\ \mathbf{c_2} \\ \vdots \\ \mathbf{c_m} \end{pmatrix}. \qquad (3.1)$$

This may be simply rewritten in the form of a standard wave variable equation

$$\mathbf{b = Sa + c} \qquad (3.2)$$

keeping in mind that $\mathbf{a}$, $\mathbf{b}$, and $\mathbf{c}$, are now composite wave vectors, and $\mathbf{S}$ is a block diagonal matrix whose submatrices along the diagonal are the scattering matrices of the components.

The connections that exist between the m elements of the network will impose constraints on components of the vectors $\mathbf{a}$ and $\mathbf{b}$. Namely, where a connection exists, there will be an equality established between incident and output waves. This is demonstrated by the waves at a single connection shown in Fig. 3.1(b). These waves must satisfy
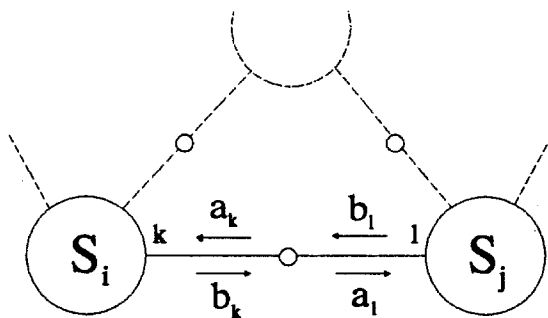
$$a_k = b_l \qquad a_l = b_k. \qquad (3.3)$$

Similar relations are apparent at every connection. This allows construction of a *connection matrix* Γ satisfying

$$\mathbf{b = \Gamma a} \qquad (3.4)$$
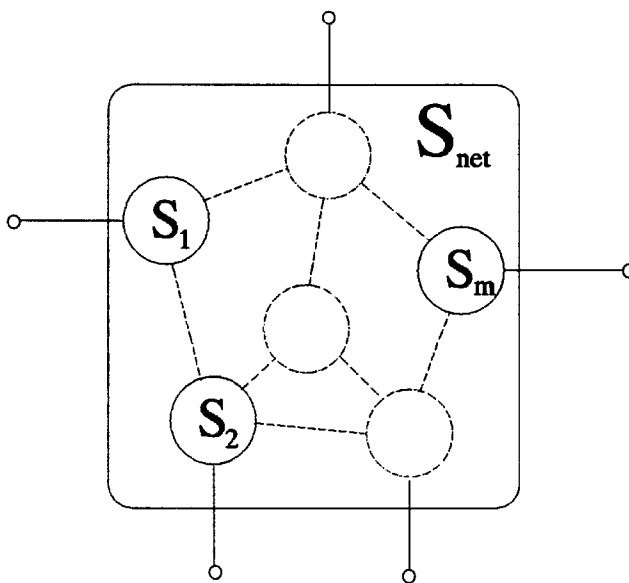
(a)

(b)

Figure 3.1 An aggregate network, S_{net}, consisting of many interconnected components, each characterized by scattering parameters. Schematic diagram of the network (a), and detail showing an incident and output wave for components S_i and S_j at a connection (b).

The components of Γ are all zeros, except those entries that correspond to a connection, and have a value of unity. Application of (3.2) and (3.4) gives the solution for the output wave vector [1]

$$b = \Gamma(\Gamma - S)^{-1}c. \qquad (3.5)$$

The composite network is therefore solved solely in terms of the component S-matrices and knowledge of the interconnections. This is a brute-force method. The $(\Gamma - S)$ matrix, albeit sparse [2], can be quite large, and its inversion leads to long computation times. The solution (3.5) comes in terms of the composite wave vector b, giving output waves for the aggregate network, and also those for each component within the network, although the latter are generally of no concern. In addition, (3.5) cannot be applied directly to the source free $(c = 0)$ case. This type of method may be used to perform noise analysis, as recently proposed by Dobrowolski [3]. These problems, however, inspire the need for an alternative.

Improvement is possible through application of connection methods. The idea is to divide the network to be solved into subcircuits to simplify the overall calculation. Such an approach was first described by Murray-Lasso [4] using indefinite admittance matrices, and has also been described using wave variables in the absence of sources [5]. The first step is to separate internal and external variables of the network. In Fig. 3.1(a), connections internal to the network S_{net} are shown with dotted lines. Those connections external to the network, and accessible by terminals, are shown in solid lines. Simplification is obtained by avoiding outright calculation of internal variables.

The process begins, as before, with tableau equation (3.1). Next, those waves which are external to the network are separated from those internal. This results in the partitioned form of (3.2):

$$\begin{pmatrix} b_e \\ b_i \end{pmatrix} = \begin{pmatrix} S_{ee} & S_{ei} \\ S_{ie} & S_{ii} \end{pmatrix} \begin{pmatrix} a_e \\ a_i \end{pmatrix} + \begin{pmatrix} c_e \\ c_i \end{pmatrix} \qquad (3.6)$$

where the external waves are denoted by subscript e, and those internal by subscript i. The topology of the network is based on connections between internal elements, so the connection matrix Γ may be redefined using

$$\mathbf{b_i} = \Gamma \, \mathbf{a_i}. \tag{3.7}$$

As before, Γ designates equality between internal incident and outward waves, so its elements are either 1 or 0 for components with consistent definitions of normalizing impedance. Desired is the scattering matrix for the aggregate network $\mathbf{S_{net}}$ defined as the ratio of external incident and outward deterministic waves, and the equivalent source wave for the network $\mathbf{c_{net}}$ that satisfy:

$$\mathbf{b_e} = \mathbf{S_{net}} \, \mathbf{a_e} + \mathbf{c_{net}}. \tag{3.8}$$

This is sufficient information to calculate the source free S-matrix for the network. Setting the source terms to zero and solving equations (3.6)–(3.8) yields the connection formula:

$$\mathbf{S_{net}} = \mathbf{S_{ee}} + \mathbf{S_{ei}}(\Gamma - \mathbf{S_{ii}})^{-1}\mathbf{S_{ie}}. \tag{3.9}$$

Solving the problem with sources included is accomplished by defining $\mathbf{c_{net}}$ as the waves that exit the network in the absence of input:

$$\mathbf{c_{net}} = \mathbf{b_e} \Big|_{\mathbf{a_e}=0} \tag{3.10}$$

leading to

$$\mathbf{c_{net}} = \begin{bmatrix} \mathbf{I} & | & \mathbf{S_{ei}}(\Gamma - \mathbf{S_{ii}})^{-1} \end{bmatrix} \begin{pmatrix} \mathbf{c_e} \\ \mathbf{c_i} \end{pmatrix} \tag{3.11}$$

where $\mathbf{I}$ is an identity matrix with order equal to the number of external ports, Γ is the same connection matrix defined by (3.7), and the bar ($|$) denotes matrix augmentation. If the source terms $\mathbf{c_e}$ and $\mathbf{c_i}$ are due to noise, then the solution must be put in terms of a noise wave correlation matrix. Using the partitioning

method of (3.6), a noise wave correlation matrix may be defined in terms of internal and external noise waves

$$C_s = \begin{pmatrix} \overline{c_e c_e^\dagger} & \overline{c_e c_i^\dagger} \\ \overline{c_i c_e^\dagger} & \overline{c_i c_i^\dagger} \end{pmatrix}. \tag{3.12}$$

This matrix is filled with values from the known noise wave correlation matrices of the components. The connection formula for the new correlation matrix is found by applying $C_{net} = \overline{c_{net} c_{net}^\dagger}$ and (3.11)

$$C_{net} = \begin{bmatrix} I & | & S_{ei}(\Gamma - S_{ii})^{-1} \end{bmatrix} C_s \begin{bmatrix} I & | & S_{ei}(\Gamma - S_{ii})^{-1} \end{bmatrix}^\dagger. \tag{3.13}$$

This result, combined with (3.9), gives a complete noise and signal characterization of the aggregate network. Several improvements have been made over the approach leading to (3.5). A direct calculation of the new scattering matrix is now possible using (3.9). In addition, the order of the matrix to be inverted has been reduced by an amount equal to the number of external ports. A very dramatic advantage also comes from the similarities in the expressions for S_{net} and C_{net}. Both share the $(\Gamma - S_{ii})^{-1}$ matrix in their calculations. It is this matrix inversion that requires most of the computational effort. Surprisingly, in approximately the same time required for performing a lone signal analysis, both signal and noise analyses may be performed.

3.2 Network Reduction by Subnetwork Growth

Unfortunately, for a circuit comprised of many components, the computer time and memory required to perform even the simpler $(\mathbf{\Gamma} - \mathbf{S}_{ii})$ matrix inversion can be prohibitive. It does tend to be a sparse matrix, however, so appropriate methods are in order. General methods have been described elsewhere [2,6], yet an alternative sparse matrix approach is available for this specific problem. Known as subnetwork growth [1], it involves a repeated application of connection formulas. Computation time is reduced by building up large networks by connecting smaller subnetworks together, two at a time, reducing the size of the matrix to be inverted. In the simple subnetwork growth procedure described here, only one connection is made at a time, reducing the size of the $(\mathbf{\Gamma} - \mathbf{S}_{ii})$ matrix to a 2-by-2. This process is illustrated in Fig. 3.2 for a branch-line coupler. The coupler is a network comprised of eight parts: four quarter-wave transmission lines, and four tees. These are labeled A through H in the figure, and the external ports are numbered from 1 to 4. In the first step, the parts are joined in pairs forming four three-port subnetworks. Next, these three-ports are combined in pairs forming the two four-ports, $ABCD$ and $EFGH$. Finally, the two four-ports are joined to make the complete branch-line coupler.

Subnetwork growth for deterministic analysis has been studied by Monaco and Tiberio [7] and Filipsson [8]. Since no intermediate results are stored, the method has a fundamental difficulty in that the entire process must be repeated for multiple analyses. However, in a comparison to a more standard sparse matrix method that included pre-processing for fast re-analysis, subnetwork growth was shown to be superior in speed for analyses numbering less than 120 [5]. Execution time is sensitive to the order in which the joints are made, so a search for the connection that results in a new subnetwork with the smallest number of parameters is needed.
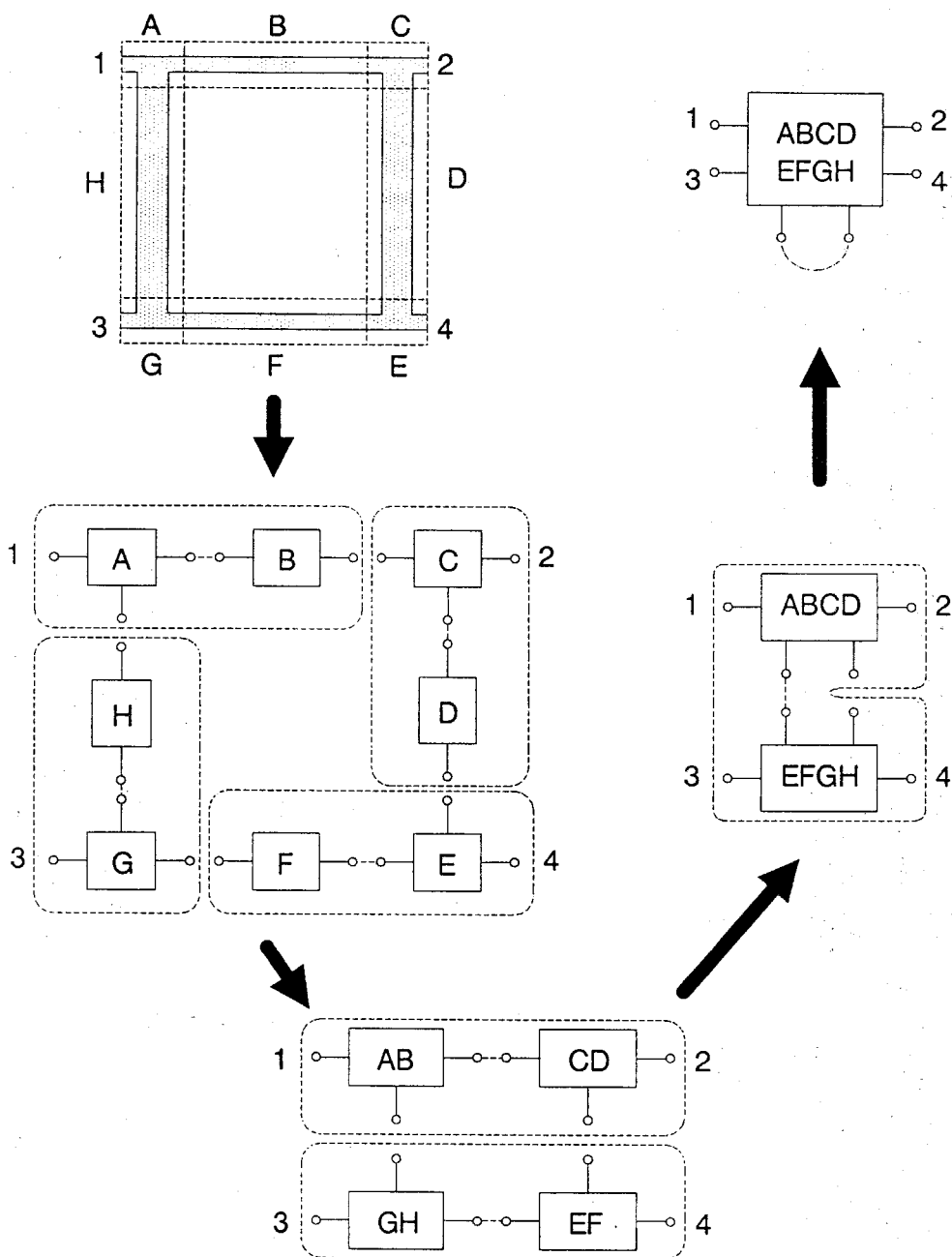
Figure 3.2 The subnetwork growth process applied to a branch-line coupler. The analysis begins with the coupler considered as eight distinct components. These are connected in pairs to form four three-port components. These, in turn, are connected in pairs, and two four-port components result. Joining the two four-ports, and then making the final connection, results in a single four-port network.

The subnetwork growth process can be applied to perform simultaneous deterministic and noise analyses. Connection formulas, equivalent to specific applications of (3.9) and (3.13), are needed to perform this task, and shall be derived using signal-flow graphs. Performing noise analysis in such a way is similar to a summation method recently described by Kanaglekar, et al. [9].

In the example of Fig. 3.2, it was evident that only two basic types of connections are needed during the subnetwork growth process. These are depicted in Fig. 3.3. Shown in Fig. 3.3(a) is the intra-connection. This occurs when two ports of the same network must be combined, resulting in a reduced number of ports. Shown in Fig. 3.3(b) is the inter-connection. This is used to combine ports of two different networks, resulting in a reduced number of subnetworks. Separate intra- and inter-connection formulas are needed for deterministic and noise analyses. Those required for the deterministic case shall be examined first.

Given in Fig. 3.4 is the reference diagram and corresponding signal-flow graph for the deterministic intra-connection. This graph, and those that follow, are independent of the number of ports possessed by the networks being reduced. Indices k and l denote the ports being reduced by the intra-connection. Indices i and j denote any two other ports possessed by the multiport **S**. Solving the signal-flow graph gives an expression for the new scattering parameters modified by the connection:

$$s'_{ij} = s_{ij} + \frac{s_{kj}s_{il}(1 - s_{lk}) + s_{lj}s_{ik}(1 - s_{kl}) + s_{kj}s_{ll}s_{ik} + s_{lj}s_{kk}s_{il}}{(1 - s_{kl})(1 - s_{lk}) - s_{kk}s_{ll}}. \qquad (3.14)$$

The indices i and j are varied over each of the other ports to generate a new scattering matrix. If the initial order of the square scattering matrix **S** was n, the process reduces it to order $n - 2$.

Given in Fig. 3.5 is the reference diagram and corresponding signal-flow graph for the deterministic inter-connection. Indices k and l again denote the
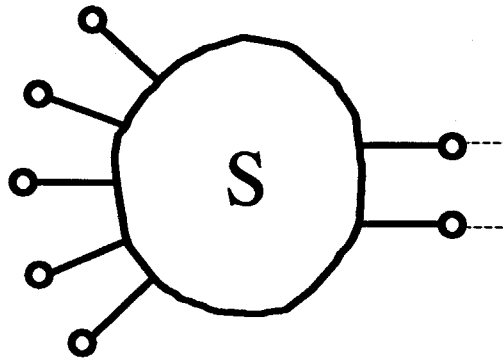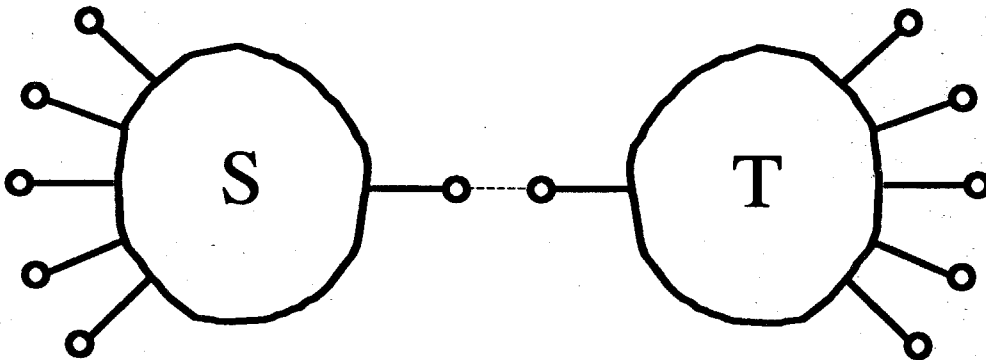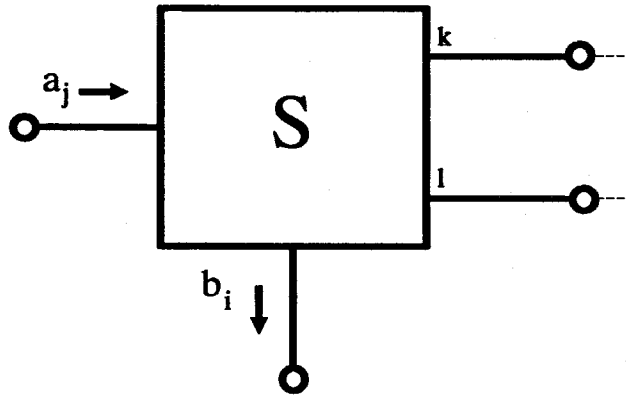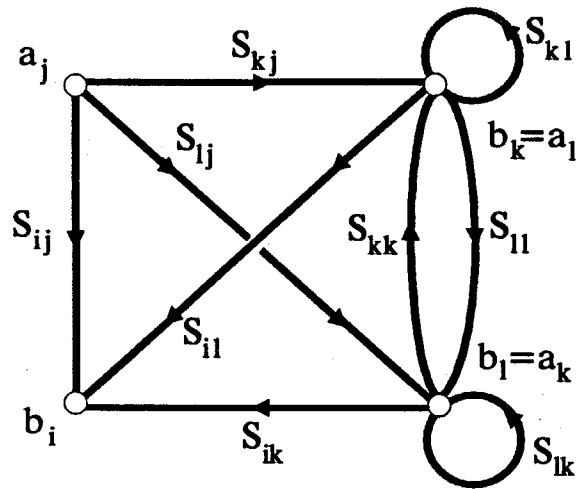
Figure 3.3 The two basic types of connections that occur during the subnetwork growth process: (a) the intra-connection, (b) the inter-connection.

(a)

(b)

Figure 3.4 Reference connection diagram (a) and signal-flow graph (b) for the deterministic intra-connection. The network **S** is an arbitrary multiport with indices i and j denoting any two ports other than the joined ports k and l.

ports being reduced. Indices i, j, and m denote other ports possessed by **S** and **T**. Solving the signal-flow graph gives

$$s'_{ij} = s_{ij} + \frac{s_{kj}t_{ll}s_{ik}}{1 - s_{kk}t_{ll}} \tag{3.15a}$$

$$s'_{mj} = \frac{s_{kj}t_{ml}}{1 - s_{kk}t_{ll}}. \tag{3.15b}$$

The indices are again varied over all ports other than k and l, resulting in a single subnetwork scattering matrix. If original scattering matrices **S** and **T** had order n and m, respectively, then the new combined matrix will have order $n + m - 2$.

A subnetwork growth procedure, using the connection formulas given above, has been implemented in the microwave computer-aided design program named *PUFF* [10]. Using the three connection formulas from (3.14) and (3.15), optimized for speed, the equivalent of the matrix inversion of (3.9) is performed. Linked lists are used in the program to keep track of components and connections. To perform the analysis, *PUFF* collapses the lists by repeatedly forming intermediate subnetworks using single connections. When every connection has been made, the complete network has been formed. The success of the *PUFF* implementation [11,12] has inspired a similar procedure for performing noise analysis to simplify (3.13). Given in Fig. 3.6 is the reference diagram and corresponding signal-flow graph for the noisy intra-connection. Indices are used as before, and also designate the outward directed noise waves present at each port. The signal-flow graph is different from that in Fig. 3.4, and now contains only those nodes and branches that result in changes to the noise waves. Solving the graph gives

$$c'_i = c_i + \frac{c_l[s_{ik}(1 - s_{kl}) + s_{kk}s_{il}] + c_k[s_{il}(1 - s_{lk}) + s_{ll}s_{ik}]}{(1 - s_{kl})(1 - s_{lk}) - s_{kk}s_{ll}} \tag{3.16a}$$

$$c'_j = c_j + \frac{c_l[s_{jk}(1 - s_{kl}) + s_{kk}s_{jl}] + c_k[s_{jl}(1 - s_{lk}) + s_{ll}s_{jk}]}{(1 - s_{kl})(1 - s_{lk}) - s_{kk}s_{ll}} \tag{3.16b}$$
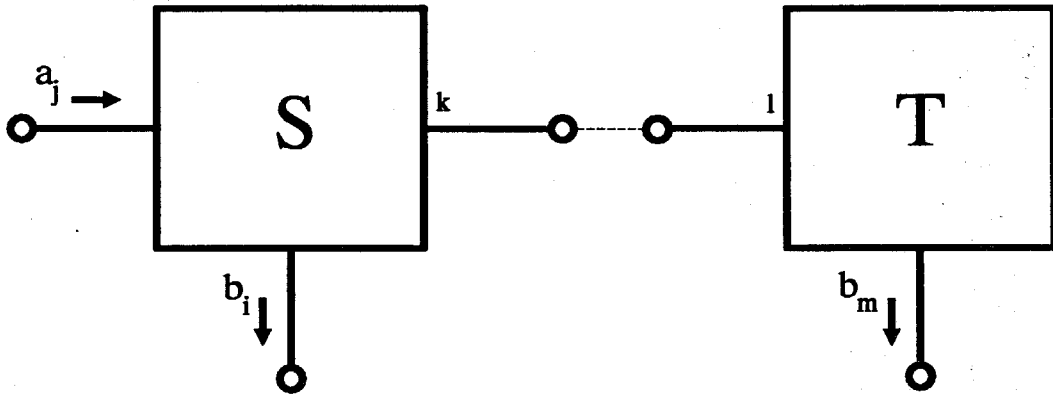
(a)
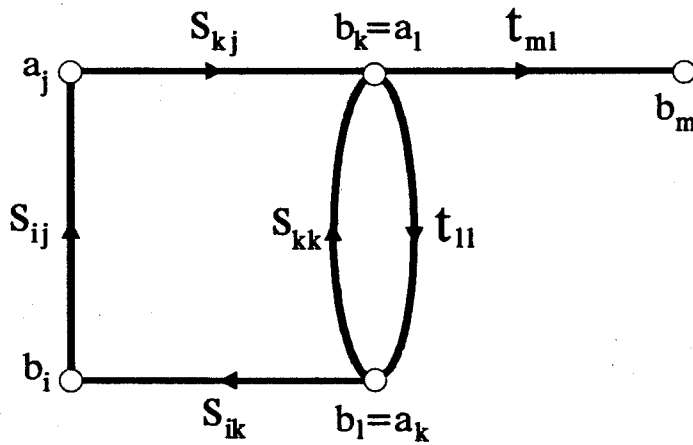
(b)

Figure 3.5 Reference connection diagram (a) and signal-flow graph (b) for the deterministic inter-connection. Networks **S** and **T** are arbitrary multiports with indices i, j, and m denoting any two ports other than the joined ports k and l.

where c_i' and c_j' are found by summing the contributions from the noise waves to nodes b_i and b_j, respectively. Since noise waves $c_i \ldots c_l$ are random variables, the above equations give no direct information. They must be related to elements of the noise correlation matrix of network **S**. This is accomplished by taking a correlation product of equations (3.16). The result is

$$\overline{c_i' c_j'^*} = \overline{c_i c_j^*} + \overline{c_l c_k^*} \frac{(s_{ik}(1 - s_{kl}) + s_{kk}s_{il})(s_{jl}(1 - s_{lk}) + s_{ll}s_{jk})^*}{|(1 - s_{kl})(1 - s_{lk}) - s_{kk}s_{ll}|^2}$$
$$+ \overline{c_k c_l^*} \frac{(s_{il}(1 - s_{lk}) + s_{ll}s_{ik})(s_{jk}(1 - s_{kl}) + s_{kk}s_{jl})^*}{|(1 - s_{kl})(1 - s_{lk}) - s_{kk}s_{ll}|^2}$$
$$+ \overline{|c_l|^2} \frac{(s_{ik}(1 - s_{kl}) + s_{kk}s_{il})(s_{jk}(1 - s_{kl}) + s_{kk}s_{jl})^*}{|(1 - s_{kl})(1 - s_{lk}) - s_{kk}s_{ll}|^2}$$
$$+ \overline{|c_k|^2} \frac{(s_{il}(1 - s_{lk}) + s_{ll}s_{ik})(s_{jl}(1 - s_{lk}) + s_{ll}s_{jk})^*}{|(1 - s_{kl})(1 - s_{lk}) - s_{kk}s_{ll}|^2}$$
$$+ \overline{c_l c_j^*} \left(\frac{s_{ik}(1 - s_{kl}) + s_{kk}s_{il}}{(1 - s_{kl})(1 - s_{lk}) - s_{kk}s_{ll}} \right) \qquad (3.17)$$
$$+ \overline{c_k c_j^*} \left(\frac{s_{il}(1 - s_{lk}) + s_{ll}s_{ik}}{(1 - s_{kl})(1 - s_{lk}) - s_{kk}s_{ll}} \right)$$
$$+ \overline{c_i c_l^*} \left(\frac{s_{jk}(1 - s_{kl}) + s_{kk}s_{jl}}{(1 - s_{kl})(1 - s_{lk}) - s_{kk}s_{ll}} \right)^*$$
$$+ \overline{c_i c_k^*} \left(\frac{s_{jl}(1 - s_{lk}) + s_{ll}s_{jk}}{(1 - s_{kl})(1 - s_{lk}) - s_{kk}s_{ll}} \right)^*.$$

As in the deterministic case, indices i and j are varied over each port to generate a new noise wave correlation matrix.

The procedure is similar for the case of the noisy inter-connection. The connection diagram and signal-flow graph are as given in Fig. 3.7. In this case, two noise wave correlation matrices, one for **S** and another for **T**, must be combined to form a solitary correlation matrix. Summing the contributions to b_i, b_j, and b_m from the signal flow graph gives

$$c_i' = c_i + \frac{s_{ik}(t_{ll}c_k + c_l)}{1 - s_{kk}t_{ll}} \qquad (3.18a)$$

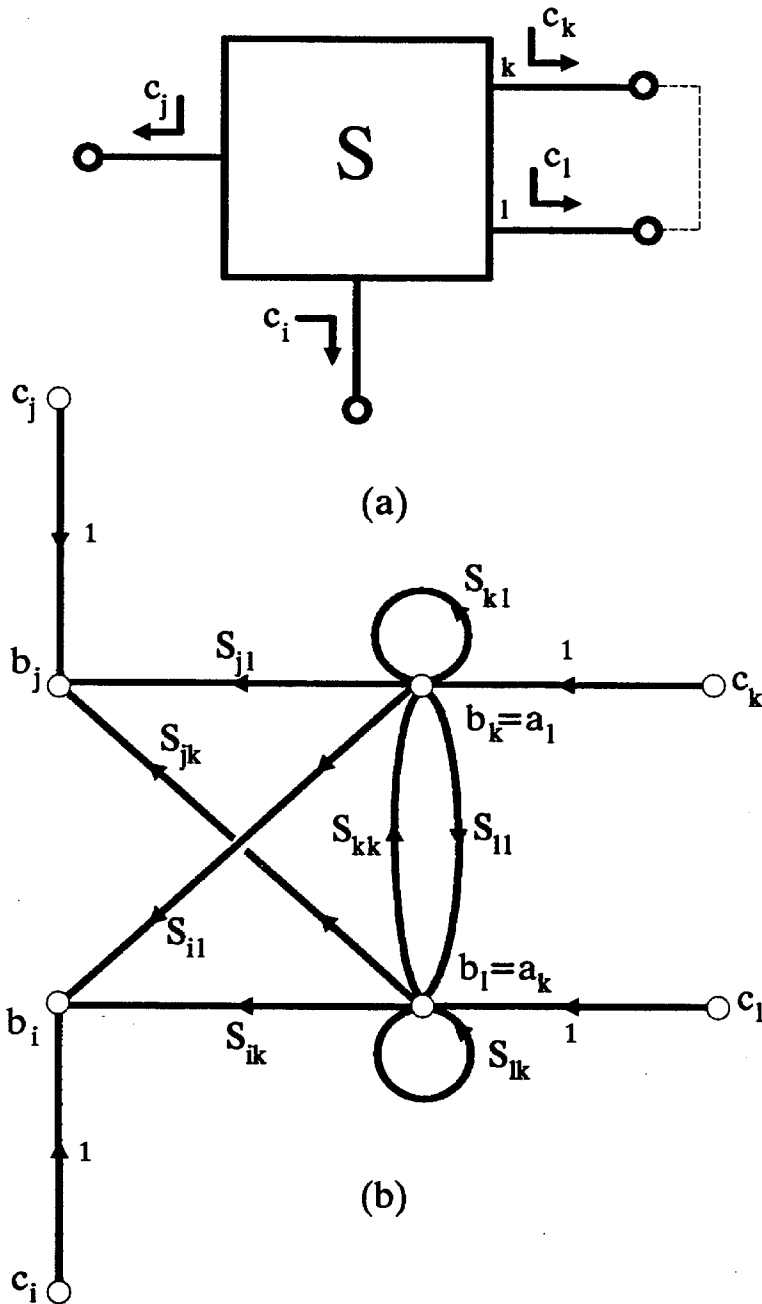$$c_j' = c_j + \frac{s_{jk}(t_{ll}c_k + c_l)}{1 - s_{kk}t_{ll}} \qquad (3.18b)$$

Figure 3.6 Reference connection diagram (a) and signal-flow graph (b) for the noisy intra-connection. The network S is an arbitrary multiport with indices i and j denoting any two ports other than the joined ports k and l.

$$c'_m = c_m + \frac{t_{ml}(s_{kk}c_l + c_k)}{1 - s_{kk}t_{ll}}. \tag{3.18c}$$

As before, correlation products of these variables must be taken, resulting in

$$\overline{c'_i c'^*_j} = \overline{c_i c^*_j} + \overline{c_i c^*_k}\left(\frac{s_{jk}t_{ll}}{1 - s_{kk}t_{ll}}\right)^* + \overline{c_k c^*_j}\left(\frac{s_{ik}t_{ll}}{1 - s_{kk}t_{ll}}\right)$$
$$+ \frac{s_{ik}s^*_{jk}}{|1 - s_{kk}t_{ll}|^2}\left(\overline{|c_l|^2} + |t_{ll}|^2\overline{|c_k|^2}\right) \tag{3.19a}$$

$$\overline{c'_m c'^*_j} = \overline{c_m c^*_l}\left(\frac{s_{jk}}{1 - s_{kk}t_{ll}}\right)^* + \overline{c_k c^*_j}\left(\frac{t_{ml}}{1 - s_{kk}t_{ll}}\right)$$
$$+ \frac{t_{ml}s^*_{jk}}{|1 - s_{kk}t_{ll}|^2}\left(s_{kk}\overline{|c_l|^2} + t^*_{ll}\overline{|c_k|^2}\right). \tag{3.19b}$$

As before, indices are varied over all ports other than k and l, resulting in the new noise wave correlation matrix.

The complexity of the connection formulas for noise, (3.17) and (3.19), is misleading. Many of the terms present in the equations are shared by the deterministic subnetwork growth formulas (3.14) and (3.15). Indeed, very few additional computations are required to perform noise analysis in addition to the deterministic analysis. This is a benefit of the similarity between general equations (3.9) and (3.13).
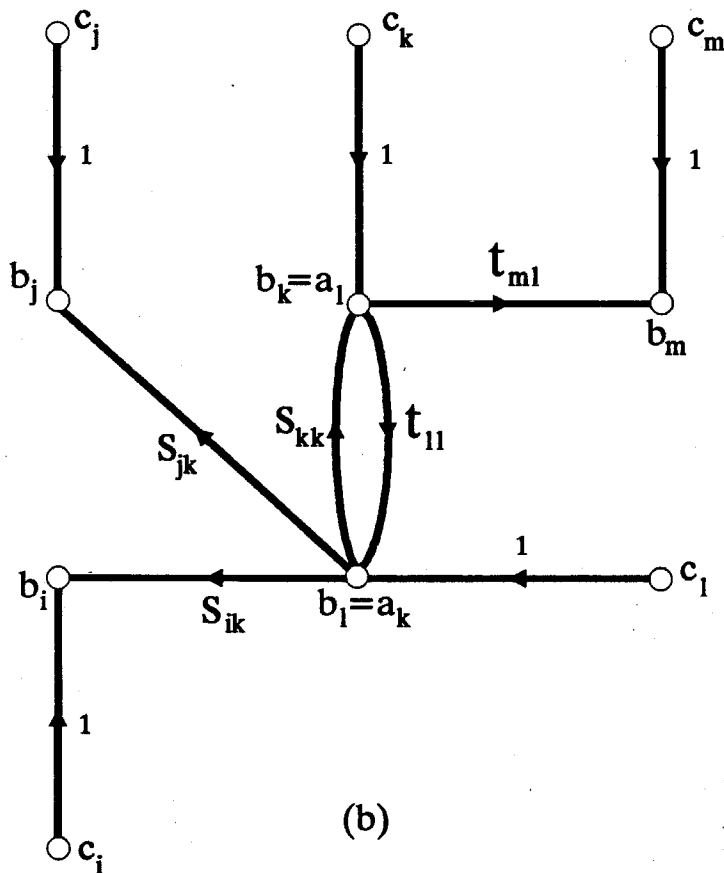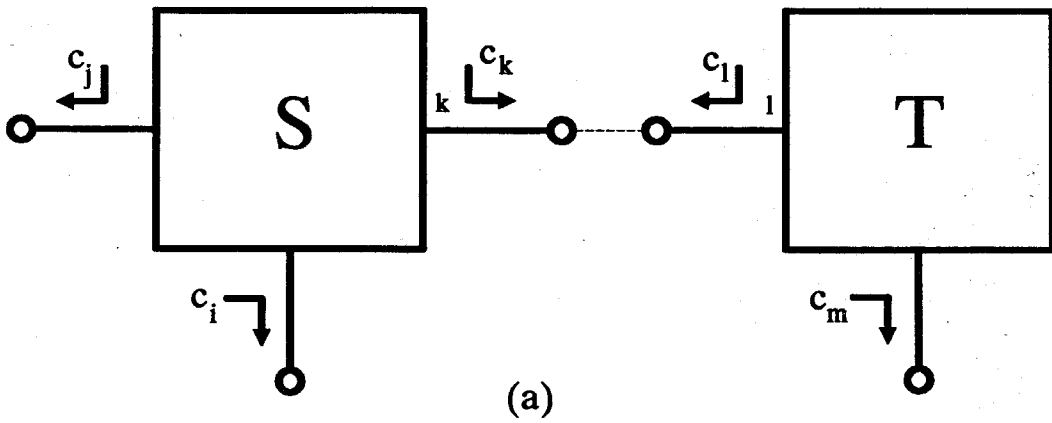
Figure 3.7 Reference connection diagram (a) and signal-flow graph (b) for the noisy inter-connection. Networks **S** and **T** are arbitrary multiports with indices i, j, and m denoting any two ports other than the joined ports k and l.

3.3 Embedded Network Connections

Connection formulas different from those derived in the previous sections result when a network is embedded entirely within another. This case is illustrated in Fig. 3.8, where a multiport S with noise wave correlation matrix C_s is embedded entirely within a network T with correlation matrix C_t. The objective is to find the resulting scattering and correlation matrices S_{net} and C_{net}.

The procedure is similar to that followed in section 3.1. First, the embedding network T is partitioned such that

$$T = \begin{pmatrix} T_{ee} & T_{ei} \\ T_{ie} & T_{ii} \end{pmatrix} \tag{3.20}$$

where subscripts e and i denote a reference to external and internal waves, respectively. The internal waves are those shared at connections between networks S and T. The external waves are those seen at the S_{net} terminals. The components of this partitioned matrix will satisfy

$$\begin{pmatrix} b_e \\ b_i \end{pmatrix} = \begin{pmatrix} T_{ee} & T_{ei} \\ T_{ie} & T_{ii} \end{pmatrix} \begin{pmatrix} a_e \\ a_i \end{pmatrix} + \begin{pmatrix} c_e \\ c_i \end{pmatrix} \tag{3.21}$$

where a are incident, b are output, and c are outward noise waves, present at either internal (i) or external (e) ports relative to T. Noise waves c_s and c_{net} are now defined as those produced by network S and S_{net}, and used to define the noise wave correlation matrices $C_s = \overline{c_s c_s^\dagger}$ and $C_{net} = \overline{c_{net} c_{net}^\dagger}$. Matrices S and S_{net} will satisfy

$$a_i = S\, b_i + c_s \tag{3.22a}$$

$$b_e = S_{net} a_e + c_{net}. \tag{3.22b}$$

Setting the noise waves to zero in (3.20)-(3.22) allows solution of the deterministic matrix

$$S_{net} = T_{ee} + \Lambda\, S\, T_{ie} \tag{3.23}$$
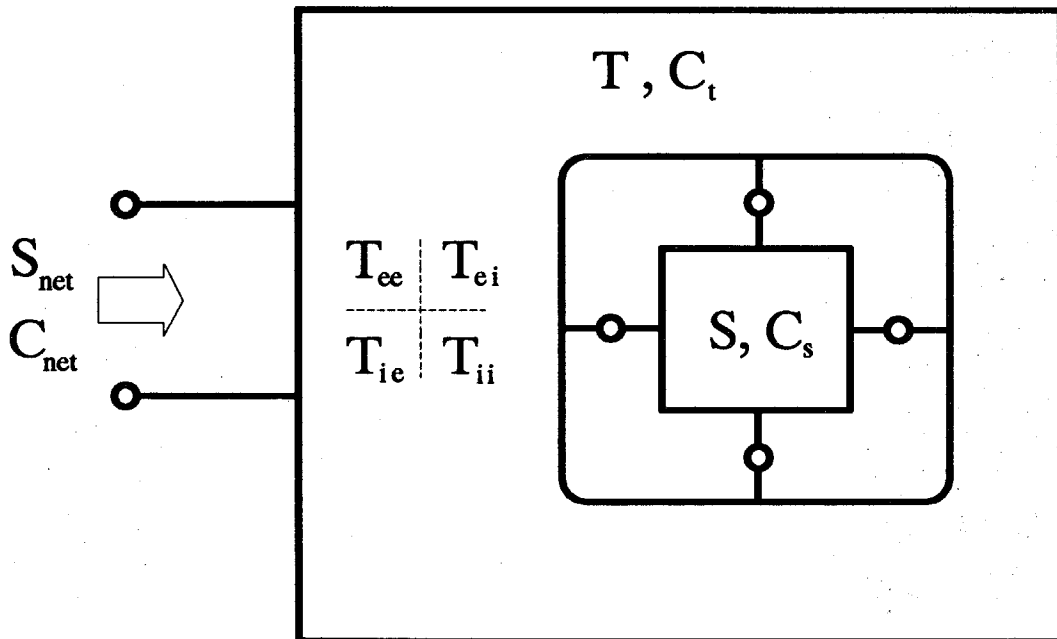
Figure 3.8 A multiport network S with noise wave correlation matrix C_s embedded within network T with correlation matrix C_t. The result of the embedding is scattering and correlation matrices S_{net} and C_{net}. Network T is partitioned in the manner shown, where subscript e denotes reference to an external wave, and i denotes reference to an internal wave. Internal waves are defined as those shared at the connections between T and S.

where

$$\Lambda = \mathbf{T_{ei}}\,(\mathbf{I} - \mathbf{S}\,\mathbf{T_{ii}})^{-1} \tag{3.24}$$

and $\mathbf{I}$ is the identity matrix. Invoking (3.10) leads to a solution for the new noise wave correlation matrix

$$\mathbf{C_{net}} = \Lambda\,\mathbf{C_s}\,\Lambda^{\dagger} + \left[\,\mathbf{I}\ \middle|\ \Lambda\mathbf{S}\,\right]\,\mathbf{C_t}\,\left[\,\mathbf{I}\ \middle|\ \Lambda\mathbf{S}\,\right]^{\dagger} \tag{3.25}$$

where, as before, a bar ($|$) is used to designate matrix augmentation.

As in section 3.1, there are similarities in the expressions for $\mathbf{S_{net}}$ and $\mathbf{C_{net}}$ that can lead to computational advantage, especially since the matrix inversion required for Λ is shared by each. Since it is possible to interpret any network as a series of embeddings, connection formulas (3.23) and (3.25) may be used for the entire computer-aided analysis process. Such an approach using admittance matrices has been described by Rizzoli and Lipparini [13]. However, expressions (3.9) and (3.13) are generally simpler to evaluate, especially using subnetwork growth. The embedding equations here have proven to be more useful in analyzing the effects of adding parasitics to a network.

References

[1] K.C. Gupta, R. Garg, and R. Chadha, *Computer–Aided Design of Microwave Circuits*, Artech House, Norwood, Massachusetts, 1981.

[2] F. Bonfatti, V. A. Monaco, and P. Tiberio, "Microwave circuit analysis by sparse-matrix techniques," *IEEE Trans. Microwave Theory Tech.*, vol. MTT-22, pp. 264-269, Mar. 1974.

[3] J.A. Dobrowolski, "A CAD–oriented method for noise figure computation of two-ports with any internal topology," *IEEE Trans. Microwave Theory Tech.*, vol. MTT-37, pp. 15-20, Jan. 1989.

[4] M.A. Murray-Lasso, "Black-box models for linear integrated circuits," *IEEE Trans. Educ.*, vol. E-12, pp. 170-180, Sept. 1969.

[5] V. A. Monaco and P. Tiberio, "Computer-aided analysis of microwave circuits," *IEEE Trans. Microwave Theory Tech.*, vol. MTT-22, pp. 249-263, Mar. 1974.

[6] S. Pissanetsky, *Sparse Matrix Technology*, Academic Press, New York, 1984.

[7] V. A. Monaco and P. Tiberio, "Automatic scattering matrix computation of microwave circuits," *Alta Freq.*, vol. 39, pp. 59-64, Feb. 1970.

[8] G. Filipsson, "A new general computer algorithm for S–matrix calculation of interconnected multiports," *Proc. 11th Euro. Microwave Conf.*, pp. 700–704, 1981.

[9] N.G. Kanaglekar, R.E. McIntosh, and W.E. Bryant, "Wave analysis of noise in interconnected multiport networks," *IEEE Trans. Microwave Theory Tech.*, vol. MTT-35, pp. 112-115, Feb. 1987.

[10] R. Compton, S. W. Wedge, and D. Rutledge, *PUFF: Computer-Aided Design for Microwave Integrated Circuits, Version 1.5*, published at Caltech, Pasadena, California, Jan. 1990.

[11] R. A. York, R. C. Compton, M. Kim, S. Wedge, and D. B. Rutledge, "An alternative approach for designing microwave circuits using a personal computer," *1988 IEEE AP-S Int. Symp. Dig.*, pp. 6-9.

[12] S.W. Wedge and D.B. Rutledge, "Computer-aided design for microwave education," *Electrosoft*, vol. 2, no. 1, Mar. 1991.

[13] V. Rizzoli and A. Lipparini, "Computer–aided noise analysis of linear multiport networks of arbitrary topology," *IEEE Trans. Microwave Theory Tech.*, vol. MTT-33, pp. 1507–1512, Dec. 1985.

Chapter 4

Component Modeling

Chapter 3 has provided methods for computing the characteristics of an aggregate network based on knowledge of its components and its connections. In a CAD program, knowledge of the connections comes essentially from bookkeeping during the generation of the layout or net-list. Each of the n-port components in a network require a representation in terms of $n \times n$ scattering and noise-wave correlation matrices. These are generally calculated from theoretical models, although it is also common to include parameters found by direct measurement.

Considerable similarity was achieved in the equations used for noise and deterministic analyses due to the compatible noise and signal representations. A similar advantage exists with components: their noise wave correlation matrices may often be calculated directly from their scattering matrices. For passive components, a simple relationship exists between the two. Referred to as Bosma's theorem, it comes readily from the principle that a passive multiport in thermodynamic equilibrium with non-reflective terminations produces uncorrelated output waves [1]. The noise generated in passive components is due to losses that give rise to thermal noise, so accurate loss modeling is desirable. For microwave transistors, deterministic modeling has long been accomplished using linear equivalent circuits. It is possible to perform noise analysis in a similar manner by assigning temperatures to resistors in the equivalent circuit to account for electronic noise in the device.

4.1 Noise Waves and Passive Components

Relationships between passive components' thermal noise and their deterministic parameters may be derived using thermodynamic arguments [2]. The simplest passive component is the one-port. It is completely characterized by a scattering parameter S and noise wave $\overline{|c|^2}$. These satisfy the scalar equation $b = Sa + c$. To solve for $\overline{|c|^2}$, the one port is terminated in the normalizing impedance Z_0, allowing no reflections. The incident wave a will be due to noise emanating from the termination, and will be uncorrelated with the noise wave c. Power flow is therefore given by $\overline{|b|^2} = |s|^2\overline{|a|^2} + \overline{|c|^2}$. With a non-reflective termination, the incident noise power $\overline{|a|^2}$ in a 1-Hz bandwidth is the available noise power kT, where k is Boltzmann's constant, T is the temperature, and quantum effects have been neglected. Thermodynamic equilibrium requires a balance in power flow such that $\overline{|a|^2} = \overline{|b|^2}$ and therefore

$$\overline{|c|^2} = kT(1 - |s|^2). \tag{4.1}$$

For the one-port, the correlation matrix is the single parameter $\overline{|c|^2}$. An equivalent to (4.1) shall now be derived for the case of an arbitrary passive multiport, beginning with the examination of a two-port passive component. In all noise calculations, a 1-Hz bandwidth will be assumed.

Shown in Fig. 4.1 is a two-port passive component **S** with reflectionless terminations. Thermodynamic equilibrium is assumed; the terminations and two-port having reached a common temperature T. Since no external sources are present, the incident waves a_1 and a_2 are due solely to the thermal noise waves emanating from the two terminations. These waves will be uncorrelated, and from the derivation of (4.1) it is known that

$$\overline{|a_1|^2} = \overline{|a_2|^2} = kT \tag{4.2a}$$

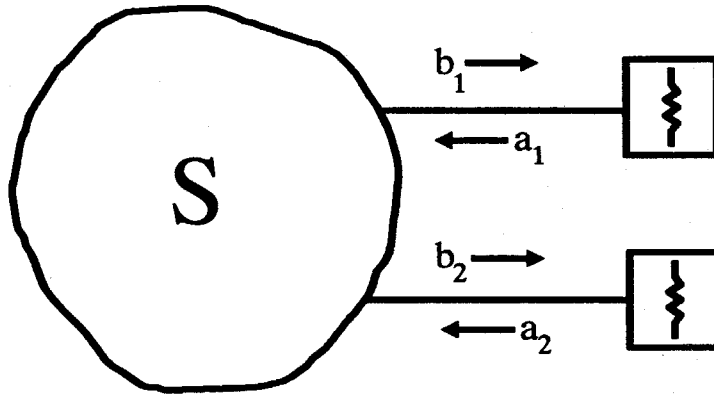$$\overline{a_2 a_1^*} = 0. \tag{4.2b}$$

Figure 4.1 A passive two-port network S with reflectionless terminations, all assumed to be at temperature T. All waves are due to thermal noise.

Thermal noise waves generated by network **S**, and the scattering of noise waves a_1 and a_2, contribute to output waves b_1 and b_2. Yet, in thermodynamic equilibrium the net power flow must be balanced, so these output waves must satisfy

$$\overline{|b_1|^2} = \overline{|b_2|^2} = kT. \tag{4.3}$$

As yet unknown is the value of the correlation product $\overline{b_2 b_1^*}$, but it may be measured. Given in Fig. 4.2 is the network of Fig. 4.1 with a directional coupler inserted between the two-port and its terminations. The primed wave variables are those that should be effected by the insertion of the coupler which is assumed to be an ideal (lossless and matched) 3-dB 180° hybrid. The effects on b_1 and b_2 are found by applying the coupler equations

$$b_1' = \tfrac{1}{\sqrt{2}}(b_1 + b_2) \tag{4.4a}$$

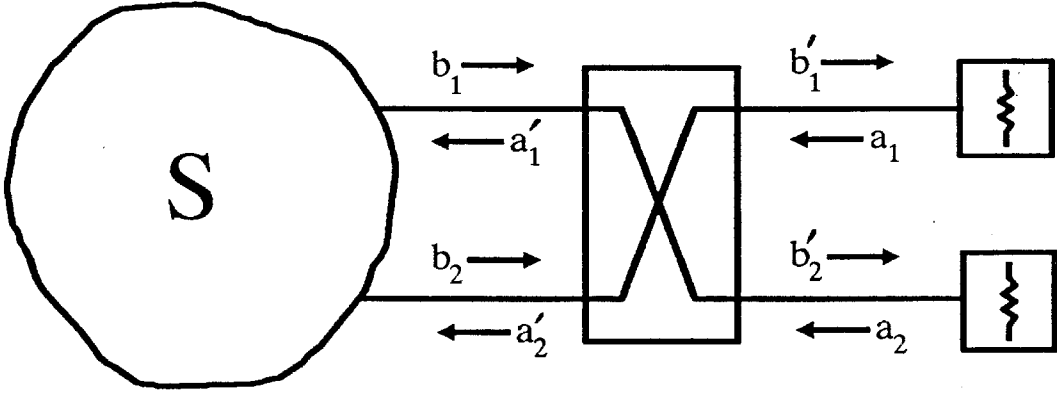$$b_2' = \tfrac{1}{\sqrt{2}}(b_1 - b_2) \tag{4.4b}$$

Figure 4.2 Directional coupler inserted between the passive two-port network S and its terminations.

resulting in

$$\overline{|b_1'|^2} = \tfrac{1}{2}\left(\overline{|b_1|^2} + \overline{|b_2|^2}\right) + Re(\overline{b_2 b_1^*}) \qquad (4.5a)$$

$$\overline{|b_2'|^2} = \tfrac{1}{2}\left(\overline{|b_1|^2} + \overline{|b_2|^2}\right) - Re(\overline{b_2 b_1^*}) \qquad (4.5b)$$

$$\overline{b_1' b_2'^*} = \tfrac{1}{2}\left(\overline{|b_1|^2} - \overline{|b_2|^2}\right) + j Im(\overline{b_2 b_1^*}). \qquad (4.5c)$$

A measure of $\overline{b_2 b_1^*}$ is possible by comparing these values. Similar expressions are obtained for a_1' and a_2', but since (4.2) remains valid for Fig. 4.2 as well as for Fig. 4.1, application of (4.5) results in

$$\overline{|a_1'|^2} = \overline{|a_2'|^2} = kT \qquad (4.6a)$$

$$\overline{a_2' a_1'^*} = 0 \qquad (4.6b)$$

demonstrating that insertion of the directional coupler has had no effect on the statistics of the noise waves originating from the terminations. Thermodynamic

equilibrium then requires that (4.3) remain valid, as well. This allows (4.5a) and (4.5b) to be simplified to

$$\overline{|b_1'|^2} = kT + Re(\overline{b_2 b_1^*}) \qquad (4.7a)$$

$$\overline{|b_2'|^2} = kT - Re(\overline{b_2 b_1^*}). \qquad (4.7b)$$

Correlation between output waves from the two-port would cause power levels other than kT to be delivered to the terminations. This would be a violation of equilibrium and cannot be the case. The continued validity of (4.2) requires that $\overline{|b_1'|^2} = \overline{|b_2'|^2} = kT$, and indeed the power in all waves must be kT. The only conclusion is that $Re(\overline{b_2 b_1^*}) = 0$.

The same reasoning may be repeated with a 3-dB 90° coupler substituted for the 180° hybrid. The result is then that $Im(\overline{b_2 b_1^*}) = 0$. The statistics of all waves considered are unaffected by the insertion of the directional couplers, leading to the conclusion that

$$\overline{b_2 b_1^*} = 0. \qquad (4.8)$$

This result is true for all passive two-ports since no restrictions other than passivity have been placed on the network.

This result can be generalized to the case of any passive multiport with reflectionless terminations described by the wave variable equation

$$\mathbf{b} = \mathbf{Sa} + \mathbf{c}. \qquad (4.9)$$

The terminations will produce uncorrelated waves with thermal noise power kT, written in vector form as

$$\overline{\mathbf{a a^\dagger}} = kT\,\mathbf{I} \qquad (4.10)$$

where $\mathbf{I}$ is the identity matrix. For the multiport, the directional coupler test can be applied to any two ports at a time. The result is the same. For any i and j, $\overline{|b_i|^2} = \overline{|b_j|^2} = kT$ and $\overline{b_i b_j^*} = 0$. As before, correlation between b_i and b_j

would result in power delivered to the loads differing from kT and is not possible. Writing this result in vector form gives

$$\overline{\mathbf{bb}^\dagger} = kT\,\mathbf{I}. \tag{4.11}$$

This lack of correlation is a rather remarkable outcome. Although input noise waves $\mathbf{a}$ will be scattered, generating correlated waves $\mathbf{Sa}$ that contribute to the output wave $\mathbf{b}$, the net correlation in the output waves must vanish. This puzzle is solved upon considering the noise wave correlation matrix for the multiport. Equation (4.11) allows a simple derivation. From (4.9)

$$\begin{aligned}
\overline{\mathbf{bb}^\dagger} &= \overline{(\mathbf{Sa} + \mathbf{c})(\mathbf{a}^\dagger \mathbf{S}^\dagger + \mathbf{c}^\dagger)} \\
&= \mathbf{S}\overline{\mathbf{aa}^\dagger}\mathbf{S}^\dagger + \overline{\mathbf{cc}^\dagger}
\end{aligned} \tag{4.12}$$

where $\overline{\mathbf{ac}^\dagger} = \overline{\mathbf{ca}^\dagger} = 0$ since the noise waves produced by a multiport and its terminations are uncorrelated. Solving for $\mathbf{C_s} = \overline{\mathbf{cc}^\dagger}$ by substitutions from (4.10) and (4.11) yields

$$\mathbf{C_s} = kT(\mathbf{I} - \mathbf{SS}^\dagger) \tag{4.13}$$

known as Bosma's theorem [3]. The noise waves contributed by the network are simply those necessary to cancel the effects of correlation present in the scattered waves $\mathbf{Sa}$ in order to maintain the lack of correlation in output waves, and to achieve balance in power flow, both required for thermodynamic equilibrium. It is well known [e.g., 4] that the fraction of power absorbed by a passive multiport is given by $(\mathbf{I} - \mathbf{S}^\dagger \mathbf{S})$; lossless networks satisfying the unitary condition $\mathbf{S}^\dagger \mathbf{S} = \mathbf{I}$. Many passive networks are reciprocal and symmetric for which $\mathbf{S}^\dagger \mathbf{S} = \mathbf{SS}^\dagger$. Equation (4.13) may be considered as a calculation of the power absorbed by the network that is available for radiation. A means is therefore provided to calculate the noise wave correlation matrix for any passive multiport in terms of its scattering matrix and temperature.

4.2 Passive Component Parameters

Models used to derive scattering parameters for most microwave components have been available for some time, although there is continual work to improve their accuracy and frequency range of validity. A distinction can be made between models for distributed microwave components: some are used for analysis, others for synthesis. In the case of analysis, the shape of the component is given and the job is to derive useful electrical parameters, such as electrical length and propagation constant. For synthesis, the desired electrical parameters are used to calculate component dimensions. Synthesis procedures used for microstrip and stripline single and coupled transmission lines have been summarized by Compton, et al. [5]. Synthesis models do not include effects due to losses and dispersion. The noise generated in passive components is due to loss, so a loss analysis must follow the synthesis procedure.

Given in Table 4.1 are the expressions used to calculate the scattering parameters for typical passive components: a two-port lumped element (lumped), a single transmission line (tline), and coupled transmission lines (clines). In the table, z is the normalized impedance, y is the normalized admittance, ℓ is the length of the component, and γ is the complex propagation constant given by

$$\gamma = \alpha + j\beta \tag{4.14}$$

where α is the attenuation factor, and β is the (real) propagation constant. In the synthesis procedure, the impedance or admittance is specified, along with the electrical length $\theta = \beta\ell$ at a specific frequency. This allows calculation of component dimensions. In analysis, the dimensions are specified, from which the impedance and electrical length must be calculated. In both cases, a calculation for the real and imaginary parts of the propagation constant γ must be made based on either given, or synthesized dimensions.

Each of the components listed in Table 4.1 is reciprocal ($s_{ij} = s_{ji}$) and symmetric ($s_{ii} = s_{jj}$). For the two-port with $\rho = s_{ii}$ and $\tau = s_{ij}$, the noise correlation matrix simplifies to:

$$\mathbf{C_s} = kT(\mathbf{I} - \mathbf{SS}^\dagger) = kT \begin{pmatrix} 1 - |\rho|^2 - |\tau|^2 & -2Re(\rho\tau^*) \\ -2Re(\rho\tau^*) & 1 - |\rho|^2 - |\tau|^2 \end{pmatrix}. \qquad (4.15)$$

Reciprocity and symmetry cause each of the terms to be real. Applying (4.15) to the lumped element of Table 4.1 gives:

$$\mathbf{C_s} = \frac{4kTRe(z)}{|z+2|^2} \begin{pmatrix} 1 & -1 \\ -1 & 1 \end{pmatrix}. \qquad (4.16)$$

A numerical advantage is seen here. For $Re(z) > 0$, the components of $\mathbf{C_s}/kT$ lie on the real line segment between $\pm\frac{1}{2}$, and stability of the matrix is ensured. In a noise voltage representation, the noise power is proportional to $4kTRe(z)$ and takes on large values at resonance. The noise wave representation gives stability comparable to the scattering parameter representation: the only unstable point is in the vicinity of $z = -2$. Negative resistance is often used to simulate parametric amplifiers, masers, and tunnel diode amplifiers. Noise generated by these devices can be modeled by assignment of a negative temperature to the device, making the diagonal components of $\mathbf{C_s}$ positive.

The calculation of the scattering matrix, and then the noise correlation matrix, for a distributed element requires knowledge of its α and β. These can be complicated functions of frequency. The models described in the following sections for dispersion and loss have been implemented in a new version of *PUFF* [6].

Part	s_{ij}
lumped	$\dfrac{z}{z+2} = \dfrac{1}{1+2y}$, for $i = j$; $\dfrac{2}{z+2} = \dfrac{2y}{1+2y}$, for $i \neq j$.
tline	$\dfrac{(z-y)\sinh\gamma\ell}{2\cosh\gamma\ell + (z+y)\sinh\gamma\ell}$, for $i = j$; $\dfrac{2}{2\cosh\gamma\ell + (z+y)\sinh\gamma\ell}$, for $i \neq j$.
clines	$\dfrac{(z_e-y_e)\sinh\gamma_e\ell}{4\cosh\gamma_e\ell+2(z_e+y_e)\sinh\gamma_e\ell} + \dfrac{(z_o-y_o)\sinh\gamma_o\ell}{4\cosh\gamma_o\ell+2(z_o+y_o)\sinh\gamma_o\ell}$, for $i = j$; $\dfrac{(z_e-y_e)\sinh\gamma_e\ell}{4\cosh\gamma_e\ell+2(z_e+y_e)\sinh\gamma_e\ell} - \dfrac{(z_o-y_o)\sinh\gamma_o\ell}{4\cosh\gamma_o\ell+2(z_o+y_o)\sinh\gamma_o\ell}$, coupled port; $\dfrac{1}{2\cosh\gamma_e\ell+(z_e+y_e)\sinh\gamma_e\ell} + \dfrac{1}{2\cosh\gamma_o\ell+(z_o+y_o)\sinh\gamma_o\ell}$, through port; $\dfrac{1}{2\cosh\gamma_e\ell+(z_e+y_e)\sinh\gamma_e\ell} - \dfrac{1}{2\cosh\gamma_o\ell+(z_o+y_o)\sinh\gamma_o\ell}$, isolated port.

Table 4.1 Expressions used to calculate the scattering parameters for common microwave passive components: a two-port lumped element (lumped), a single transmission line (tline), and coupled transmission lines (clines). In the table, z is the normalized impedance, y is the normalized admittance, γ is the complex propagation constant $\gamma = \alpha + j\beta$, and ℓ is the length of the component. The subscripts e and o refer to even and odd modes of the clines. For the clines, the ports are labeled in a way that is appropriate for a directional coupler: the through port is on the same line as the input port, but at the opposite end. The isolated port is the port diagonally across from the input, and the coupled port is at the same end as the input, but on the other line.

4.2.1 Dispersion

Microstrip is the most common microwave transmission line structure. It is inhomogeneous, causing the fundamental mode of propagation to be other than TEM. This is modeled by a relative effective dielectric constant ϵ_{re} that is a function of frequency. The real propagation constant β then follows

$$\beta(\omega) = \sqrt{\epsilon_{re}(\omega)} k_0 \qquad (4.17)$$

where k_0 is the TEM propagation constant for the equivalent transmission line with an air dielectric $k_0 = \omega\sqrt{\epsilon_0 \mu_0}$. Typically, as frequency is increased, ϵ_{re} increases in a non-linear manner, approaching an asymptotic value. For single and coupled microstrip transmission lines, ϵ_{re} may be modeled using Getsinger's expression [7,8]

$$\epsilon_{re_i}(\omega) = \epsilon_r - \frac{\epsilon_r - \epsilon_{re_i}(0)}{1 + F_i(\omega)} \qquad (4.18)$$

where ϵ_r is the relative dielectric constant of the substrate material, $\epsilon_{re_i}(0)$ is the low frequency quasi-static value, and $F_i(\omega)$ is an increasing function of frequency. The subscript i is used to distinguish between the functions and values used for single microstrip, and for even and odd modes in coupled microstrip. Accurate closed form expressions for $F_i(\omega)$ are complicated, and have been given for single and coupled microstrip transmission lines by Kirschning and Jansen [9,10]. Dispersion affects characteristic impedances in a similar way. It is modeled using Bianco's expression [11]

$$Z_{0_i}(\omega) = Z_{0_i}^s - \frac{Z_{0_i}^s - Z_{0_i}(0)}{1 + F_i(\omega)} \qquad (4.19)$$

where $Z_{0_i}^s$ is twice the characteristic impedance of an equivalent (single or coupled) stripline with twice the thickness of the microstrip, and $Z_{0_i}(0)$ is the quasi-static impedance. The functions $F_i(\omega)$ used in (4.19) are the same as those used in (4.18).

4.2.2 Losses

For distributed components with propagation constants given by (4.14), C_s takes on nonzero values when the attenuation factor α is nonzero. This loss factor includes contributions from a dielectric attenuation factor α_d and a conductor attenuation factor α_c where

$$\alpha = \alpha_c + \alpha_d. \tag{4.20}$$

The calculations for conductor attenuation have the similar form given by

$$\alpha_c^i = \frac{R_s}{Z_i W_t} K_i F_{sr} \tag{4.21}$$

where Z_i is the line impedance (even or odd mode for couplers), W_t is the effective width of the line (taking into account finite strip thickness), and K_i is the current distribution factor. The subscript and superscript i again designates differences for a single line, and even and odd modes in a coupled line. The surface resistance R_s is given by

$$R_s = \sqrt{\frac{\pi f \mu}{\sigma}} \tag{4.22}$$

at frequency f, permeability μ, and conductivity σ. The substrate surface roughness factor F_{sr} has been evaluated by Hammerstad and Bekkadal [12]. They find it well approximated by the expression

$$F_{sr} = 1 + \frac{2}{\pi} \arctan \left\{ 1.4 \left(\frac{\Delta}{\delta_s} \right)^2 \right\} \tag{4.23}$$

where Δ is the rms surface roughness and δ_s is the skin depth at the operating frequency. This factor is necessary to account for an asymptotic increase seen in the apparent surface resistance with decreasing skin depth. Expressions for the current distribution factor K_i have been given by Pucel, et al. [13] and Gupta, et al. [14] for single microstrip. Expressions for coupled microstrip have been given by Garg and Bahl [15] and Hammerstad and Jensen [16]. In most cases, K_i is derived from an application of Wheeler's incremental inductance rule [17].

Accounting for dielectric loss is done by including the effects of finite loss tangent $\tan \delta$. For the inhomogeneous line, an effective dielectric filling fraction is used to give that proportion of the transmission line's cross section not filled by air. For microstrip lines, the result is [18,19]

$$\alpha_d^i = \frac{\pi \epsilon_r}{\epsilon_r - 1} \frac{\epsilon_{re_i} - 1}{\sqrt{\epsilon_{re_i}}} \frac{\tan \delta}{\lambda_0} \qquad (4.24)$$

where again i has been used to distinguish between values for single and coupled lines. For the homogeneous transmission line, (4.24) simplifies to its well known value

$$\alpha_d = \frac{\pi \sqrt{\epsilon_r} \tan \delta}{\lambda_0}. \qquad (4.25)$$

The attenuation factors typically exhibit regular behavior; conductor loss increasing as the square root of frequency, dielectric loss increasing proportionately. In a dispersive line, the changes in impedance and dielectric constant affect (4.21) and (4.24), and can lead to more complicated behavior.

4.2.3 Quality Factor

The definition of the quality factor, or Q, for a transmission line is the same as with other components. It is the well known figure of merit for the ratio of stored energy to dissipated energy. In terms of group velocity, it is written [20]

$$Q = \omega \frac{\text{energy per unit length}}{\text{power loss per unit length}} = \frac{\omega P / v_g}{P_L} = \frac{\omega}{2 v_g \alpha} \qquad (4.26)$$

where P_L is the power loss per meter, and power flow P equals the product of the energy density and the energy transport (group) velocity v_g. Dispersion affects the group velocity according to

$$v_g = \frac{1}{d\beta / d\omega} = \frac{c / \sqrt{\epsilon_{re}(\omega)}}{1 + \dfrac{\omega}{2} \dfrac{d \ln \epsilon_{re}(\omega)}{d\omega}}. \qquad (4.27)$$

The quality factor for the dispersive line is therefore given by

$$Q = \frac{\beta}{2\alpha} \left(1 + \frac{\omega}{2} \frac{d \ln \epsilon_{re}(\omega)}{d\omega} \right).$$ (4.28)

This expression often results in complicated frequency dependencies. In the absence of dispersion, Q becomes the widely used expression

$$Q = \frac{\beta}{2\alpha}.$$ (4.29)

This has much simpler frequency behavior. In a line dominated by dielectric loss, both β and α will increase proportionately to frequency, and the Q is therefore constant. For the line dominated with conductor loss, both α and Q have $\sqrt{f}$ behavior.

The quality factor is useful in evaluating the effects of loss on the generation of noise waves. Values for the noise wave correlation matrix, derived using (4.15), (4.29), and the equations from Table 4.1, are given in Figs. 4.3 and 4.4 for a constant Q transmission line at temperature T_0. Plots in each figure are with respect to length in wavelengths (ℓ/λ). The transmission line used has normalized impedance $z = 2$, and values have been plotted for discrete Q values from 5 to 100. The normalized noise wave power ($\overline{|c_1|^2}/kT_0$), plotted in Fig. 4.3, is seen to increase steadily with electrical length. Periodic bumps in the plot are due to impedance mismatches in the line that modulate the available noise power. With increasing Q values, the behavior is similar, but the reduced loss lowers noise production. The normalized correlation ($\overline{c_1 c_2^*}/kT_0$) is plotted in Fig. 4.4. At a quarter wavelength, and every half wavelength thereafter, the correlation is seen to vanish. This occurs at frequencies where s_{21} is imaginary and s_{11} is real, resulting in orthogonality between the noise waves. Two competing effects control the envelope of the correlation plots. The lower Q's have noise waves of larger magnitude, and initially give higher correlation peaking every half wavelength where both s_{21} and s_{11} are real. Yet, as electrical length is increased,

transmission losses become so large that eventually the line looks like a single resistive termination. When this occurs, correlation vanishes. The plot for $Q = 5$ therefore has the highest first peak, yet the peaking diminishes with electrical length due to the line loss. The second positive peak ($\ell = 1.5\lambda$) is the highest for $Q = 10$. The electrical length has increased enough to make the noise more pronounced, yet is small enough to allow transmission. The highest third positive peak ($\ell = 2.5\lambda$) is for $Q = 20$. The higher Q values have steadily increasing peaking, indicating that transmission losses have yet to have an effect. For a matched transmission line ($z = 1$) no internal reflections are present and there is no correlation. The basic correlation behavior described above, however, is demonstrated by all other lossy transmission lines. Consequently, it is important to include correlation effects for even passive circuit noise calculations.

4.3 Active Device Modeling

The two most commonly used active devices for low noise microwave amplification are the gallium arsenide field effect transistor (GaAs FET) and the high electron mobility transistor (HEMT). Small-signal deterministic modeling of these devices is performed using linear equivalent circuits. These characterize the device for only a single bias point, but may be used to generate scattering parameters over a broad frequency range. The small-signal equivalent circuit used for chip form microwave GaAs FET's and HEMT's is given in Fig. 4.5.

Conventional methods for noise modeling of these devices have been summarized by Cappy [21]. In addition to the equivalent circuit, they require the determination of three dimensionless quantities that are proportional to values of a low frequency noise current correlation matrix

$$\mathbf{C_i} = \begin{pmatrix} \overline{i_g^2} & \overline{i_g i_d^*} \\ \overline{i_d i_g^*} & \overline{i_d^2} \end{pmatrix} \tag{4.30}$$

where subscripts g and d refer to the gate and drain of the transistor, respectively. Work has been done to develop empirical expressions for these quantities
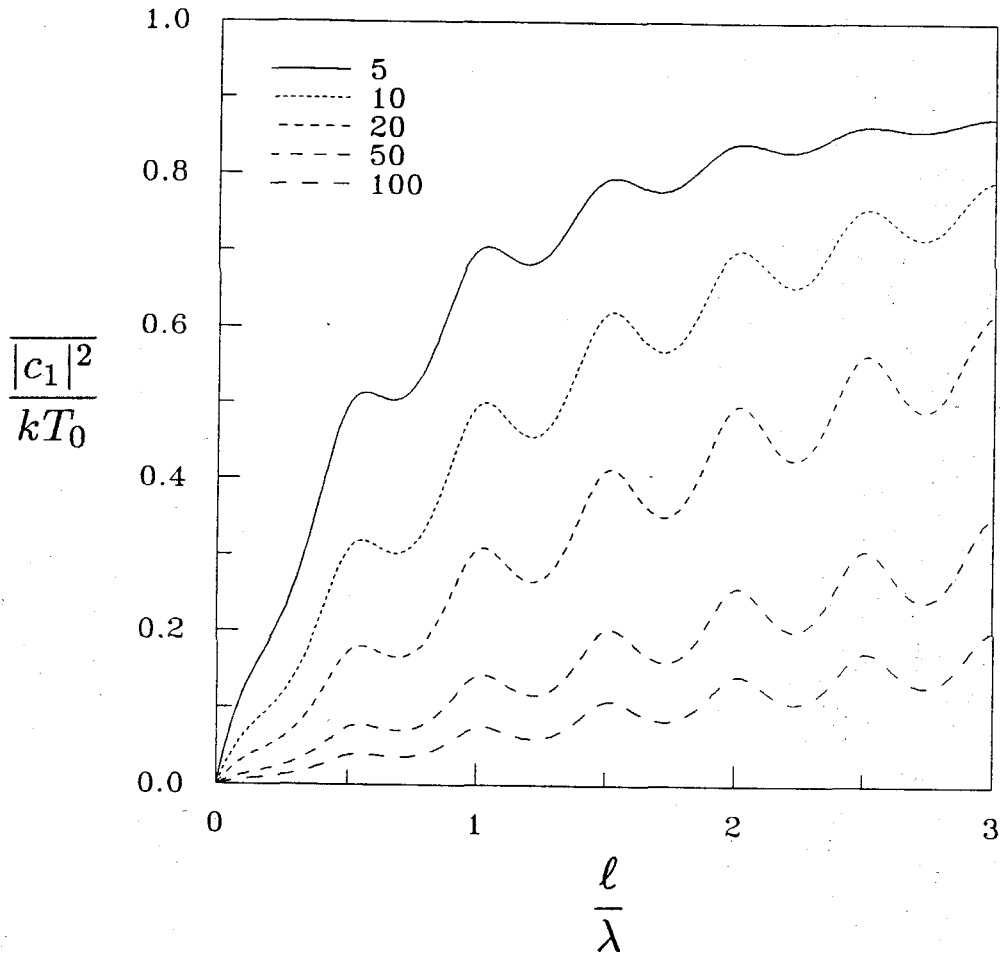
Figure 4.3 Plot of the normalized noise wave power $\overline{|c_1|^2}/kT_0$ versus length in wavelengths for a `tline` with $z = 2$. Plots are given for discrete values of Q from 5 to 100.
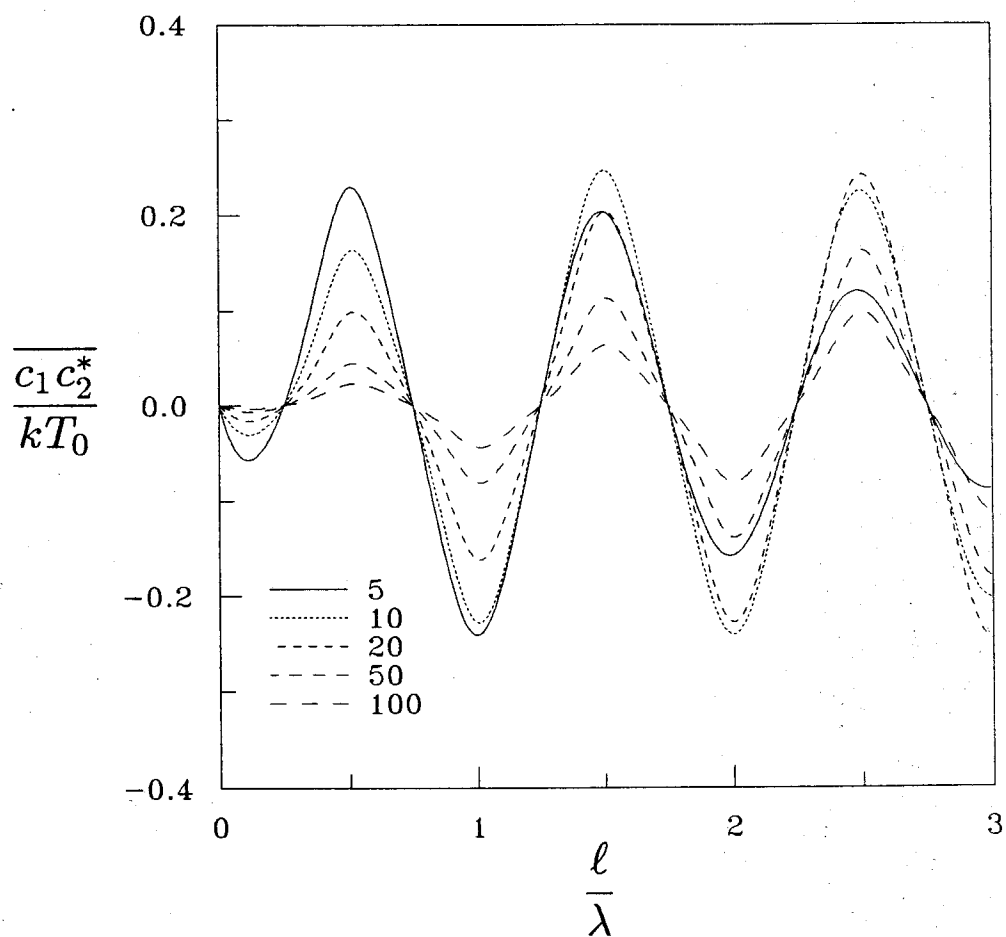
Figure 4.4 Plot of the normalized noise wave correlation $\overline{c_1 c_2^*}/kT_0$ versus length in wavelengths for a `tline` with $z = 2$. Plots are given for discrete values of Q from 5 to 100.
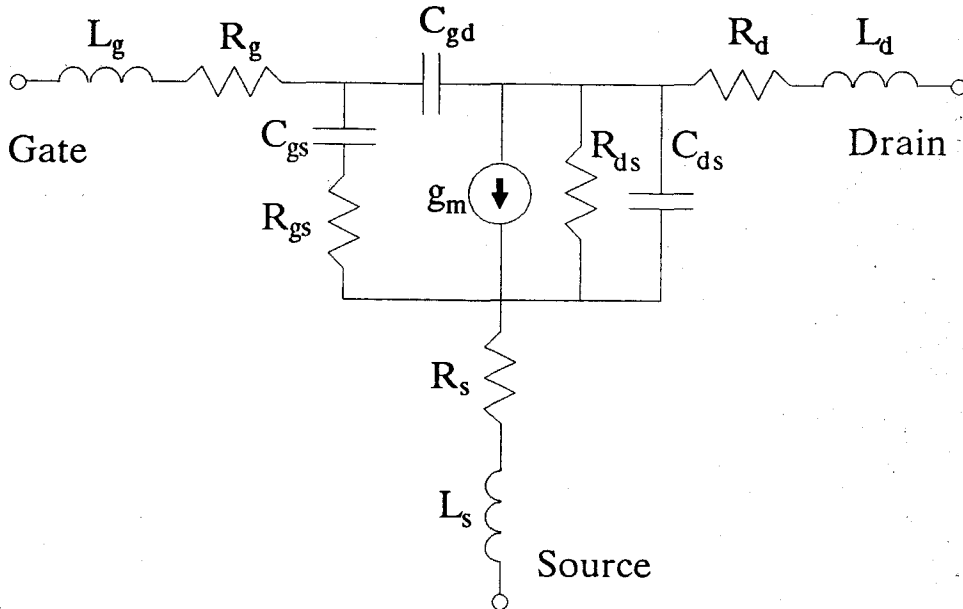
Figure 4.5 Equivalent circuit used for microwave transistors including the GaAs FET and HEMT.

in terms of material parameters [22], but the results bear no physical significance in relation to the equivalent circuit. Podell [23] first suggested that some noise information could be obtained directly from the equivalent circuit. He gave a very simple model using two uncorrelated noise sources present at the input of the device. Improvements to this model were made by Gupta, et al. [24], who obtained good results by adding correlation effects. They also showed that a frequency independent output noise current source could be used to model uncorrelated drain noise. Its value could be determined from a single low frequency spectral density measurement. Pospieszalski [25] then showed that this noise current, and indeed all values for C_i, could be modeled from the equivalent circuit by assigning temperatures to the circuit resistors to account for electronic noise.

A straightforward implementation of Pospieszalski's model is possible following the noise wave approach. The first step is to simplify the equivalent circuit

of Fig. 4.5. The gate, source, and drain leads each have a parasitic resistance and inductance that is removed. Next, the parasitic feedback capacitance C_{gd} is removed. The result is the intrinsic equivalent circuit shown in Fig. 4.6. Detail has been added showing how input voltage across capacitance C_{gs} is amplified by transconductance g_m. Also added to gate-source resistance R_{gs} and drain-source resistance R_{ds} are equivalent gate and drain temperatures T_g and T_d.

Derivation of the noise wave correlation matrix is made directly from the intrinsic equivalent circuit using the methods described earlier. With the source considered grounded, the noise waves c_1 and c_2 are considered to emanate from the gate and drain, respectively. The value of $\overline{|c_1|^2}$ is due only to the temperature and input resistance R_{gs} of the gate and is therefore given by

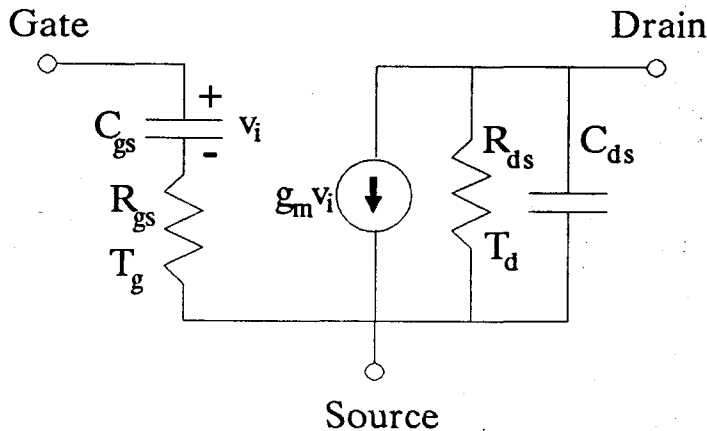$$\overline{|c_1|^2} = kT_g(1 - |s_{11}|^2). \qquad (4.31)$$

Figure 4.6 Intrinsic equivalent circuit for GaAs FET and HEMT transistors. Gate temperature T_g is the equivalent temperature of R_{gs}. Drain temperature T_d is the equivalent temperature of R_{ds}. Noise voltage generated by R_{gs} will appear at v_i and result in correlation between input and output noise waves.

Noise voltage produced by R_{gs} will appear across C_{gs}. This gate voltage is transferred to the drain, resulting in a noise correlation term given by

$$\overline{c_2 c_1^*} = \frac{s_{21}}{s_{11} - 1} \overline{|c_1|^2}. \tag{4.32}$$

For the intrinsic equivalent circuit this correlation term will be purely imaginary. The output noise power results from the correlated noise from the gate, as well as the noise present in the output resistance R_{ds} with equivalent temperature T_d, and is therefore given by

$$\overline{|c_2|^2} = \frac{|s_{21}|^2}{|1 - s_{11}|^2} \overline{|c_1|^2} + kT_d(1 - |s_{22}|^2). \tag{4.33}$$

The scattering parameters s_{11}, s_{21}, and s_{22} used in (4.30)-(4.33) may all be found from the equivalent circuit of Fig. 4.6.

As an example of noise wave modeling using the techniques developed to this point, a Fujitsu FSX02X GaAs FET and an FHR02X HEMT have been analyzed for the complete equivalent circuit of Fig. 4.5. The analysis procedure is as follows: (a) determine the scattering and noise wave correlation matrices for the intrinsic equivalent circuit (Fig. 4.6) with source lead shorted to ground; (b) convert the resulting definite matrices to indefinite forms (chapter 2); (c) use linear connection theory (chapter 3) to solve for the noise and scattering matrices for the complete equivalent circuit of Fig. 4.5; (d) convert noise wave values to standard two-port noise parameters (chapter 2). This procedure was followed using the equivalent circuit values for the GaAs FET and HEMT listed in Table 4.2. Measured noise parameter data were provided by the manufacturer and are shown here for comparison.

Given in Fig. 4.7 are Smith chart plots for theory and measurement of the optimum reflection coefficient Γ_{opt} for the Fujitsu FSX02X GaAs FET from 2-18 GHz. Agreement is exceptional. The theoretical plot was made with gate temperature $T_g = 290$ K, suggesting that this noise is truly thermal in nature.

The drain temperature used was $T_d = 1375$ K. This high value is used to simulate high-field diffusion noise and hot electron effects. Theory and measurement for the noise figure minimum F_{min} and noise resistance R_n are shown in Fig. 4.8 and Fig. 4.9, respectively. All three theoretical plots were made under the same conditions. Noise figure minimum predictions are quite good considering measurement accuracy typically on the order of 0.25 dB. Noise resistance is slightly underestimated. Given in Fig. 4.10 are Smith chart plots of modeled and measured Γ_{opt} for the Fujitsu FHR02X HEMT from 2-26 GHz. The theoretical plot was made with $T_g = 290$ K and $T_d = 1100$ K. Graphs showing comparisons of F_{min} and R_n are shown if Fig. 4.11 and Fig. 4.12, respectively. As before, predictions are quite good with the exception of R_n which deviates from theory at lower frequencies.

In the analyses above, the same equivalent circuits from which scattering parameters are derived were used to find noise wave parameters: the only additional information needed was the drain temperature for the device. Accurate predictions were obtained by assuming all other equivalent circuit components at 290 K. This is the general advantage of the noise wave approach: noise analysis, for both active and passive devices, requires knowledge of only scattering parameters and temperature.

Element	FSX02X	FHR02X
$g_{m0}(mS)$	42.5	55
$\tau(psec)$	2.0	0.85
$C_{gs}(pF)$	0.33	0.2
$C_{gd}(pF)$	0.033	0.025
$C_{ds}(pF)$	0.115	0.049
$R_{gs}(\Omega)$	3.5	2.5
$R_{ds}(\Omega)$	270.0	188.7
$R_g(\Omega)$	0.3	1.3
$R_s(\Omega)$	1.8	1.3
$R_d(\Omega)$	3.0	1.3
$L_g(nH)$	0.12	0.1
$L_s(nH)$	0.05	0.08
$L_d(nH)$	0.12	0.1
$T_g(K)$	290	290
$T_d(K)$	1375	1100

Table 4.2 Component values for elements in the equivalent circuit of Fig. 4.5 used to model the Fujitsu FSX02X GaAs FET and FHR02X HEMT. The transconductance g_m has an associated transit time τ such that $g_m = g_{m0}e^{-j\omega\tau}$. Gate temperature T_g is the equivalent temperature of R_{gs}. Drain temperature T_d is the equivalent temperature of R_{ds}. Values for both devices are for $I_{dss} = 10$ mA. The FSX02X values correspond to a bias voltage $V_{ds} = 3$ V, while $V_{ds} = 2$ V for the FHR02X.
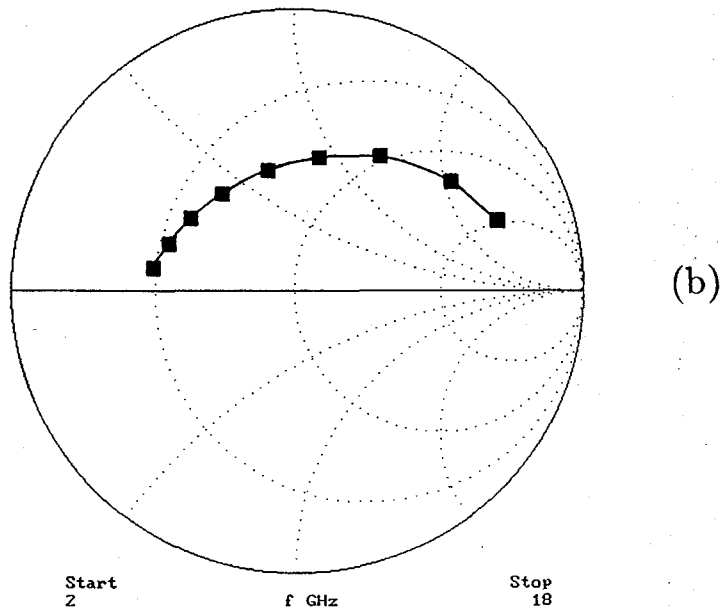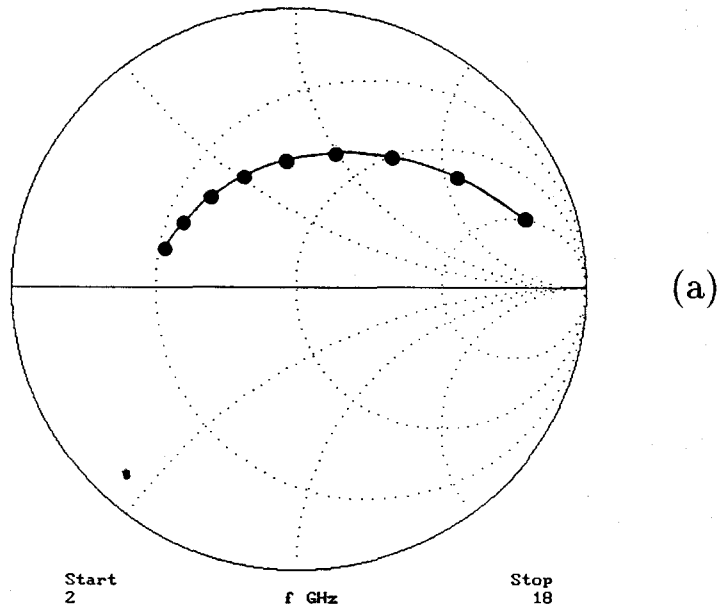
Figure 4.7 Smith chart comparison of theory (a) and measurement (b) of optimum reflection coefficient Γ_{opt} for the Fujitsu FSX02X GaAs FET. The theoretical plot was made with $T_d = 1375$ K. Plots are from 2-18 GHz, running counterclockwise over frequency, with points shown in 2 GHz increments.
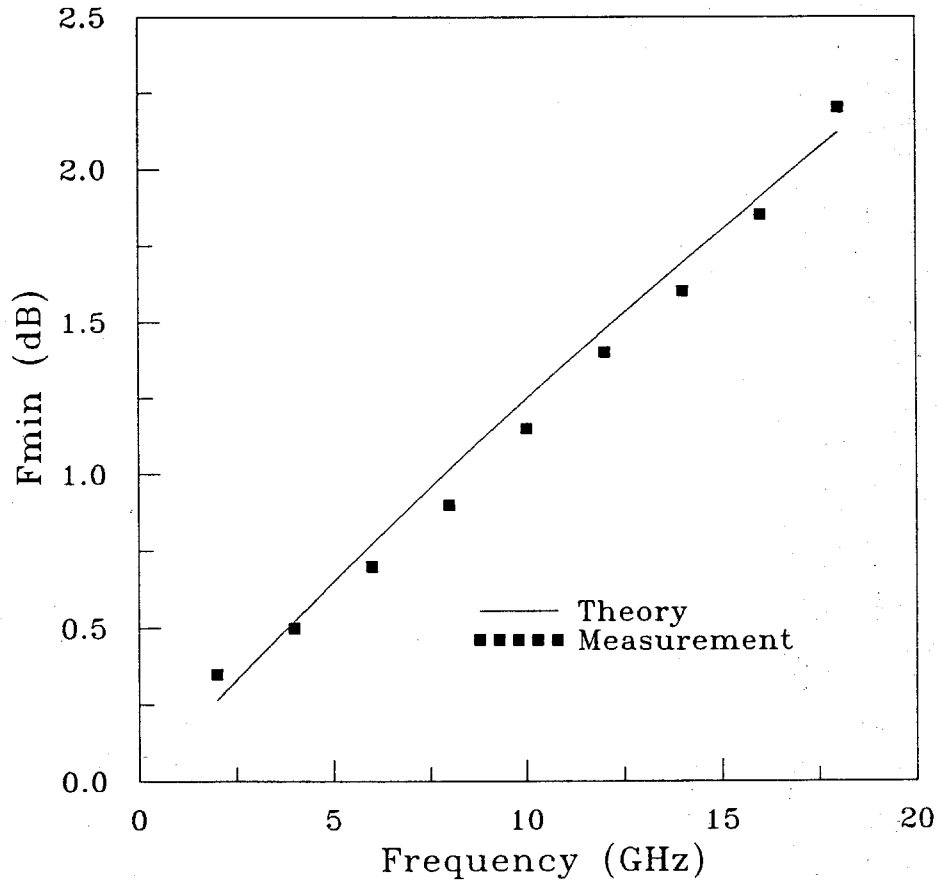
Figure 4.8 Comparison of theory and measurement of noise figure minimum F_{min} for the Fujitsu FSX02X GaAs FET. The theoretical plot was made with $T_d = 1375$ K.
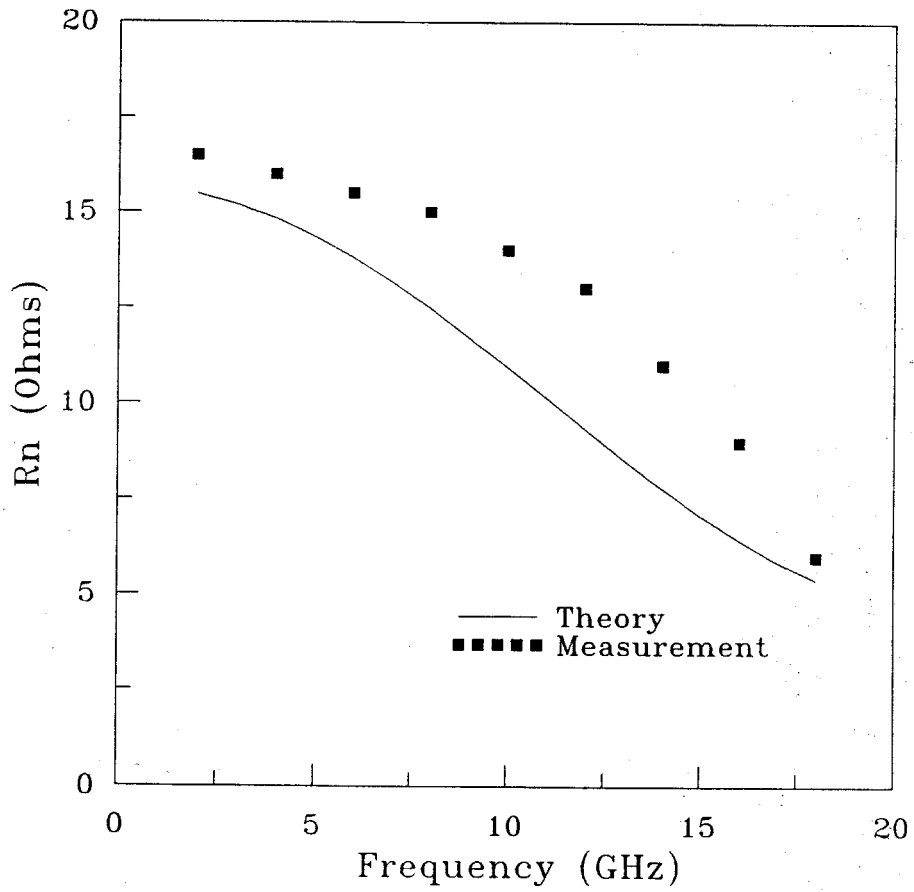
Figure 4.9 Comparison of theory and measurement of the noise resistance R_n for the Fujitsu FSX02X GaAs FET. The theoretical plot was made with $T_d = 1375$ K.
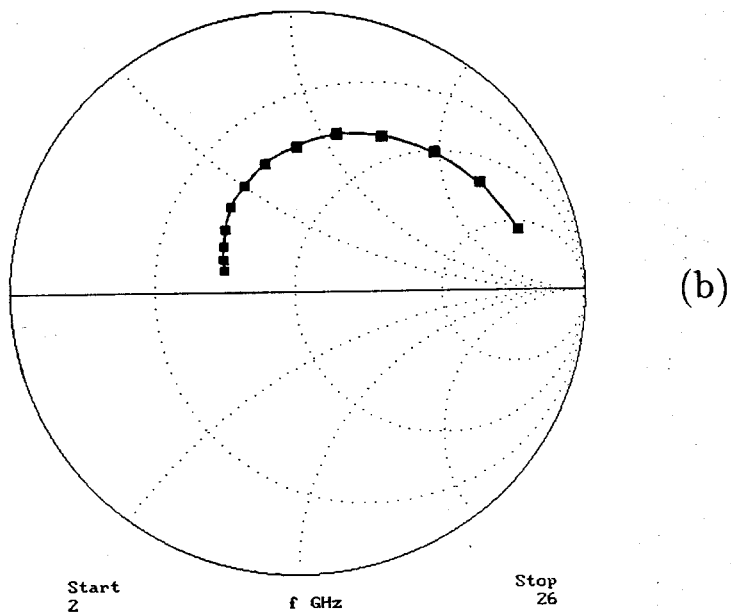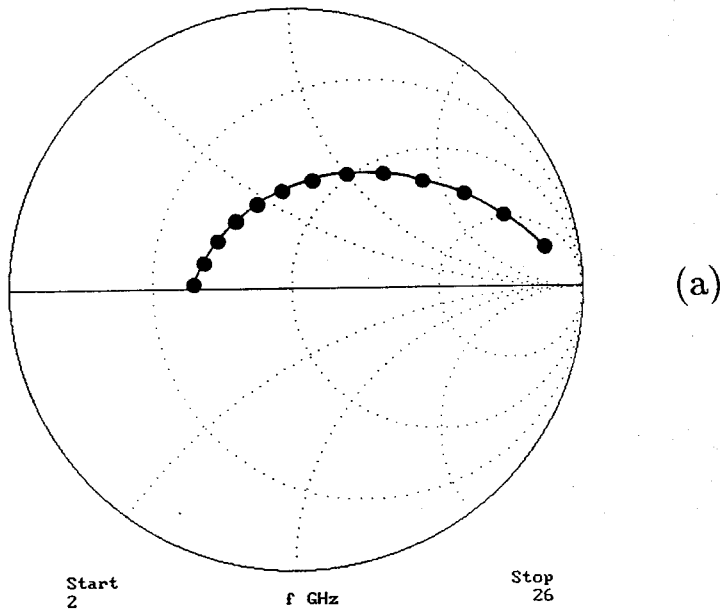
Figure 4.10 Smith chart comparison of theory (a) and measurement (b) of optimum reflection coefficient Γ_{opt} for the Fujitsu FHR02X HEMT. The theoretical plot was made with $T_d = 1100$ K. Plots are from 2-26 GHz, running counterclockwise over frequency, with points shown in 2 GHz increments.
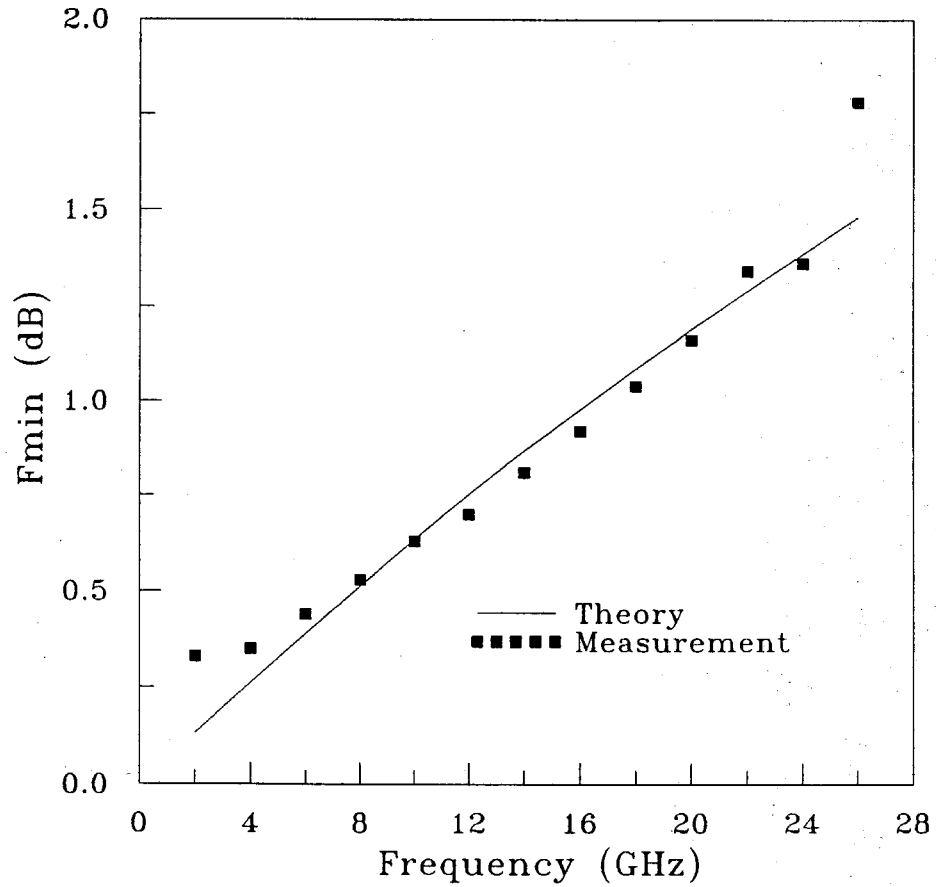
Figure 4.11 Comparison of theory and measurement of noise figure minimum F_{min} for the Fujitsu FHR02X HEMT. The theoretical plot was made with $T_d = 1100$ K.
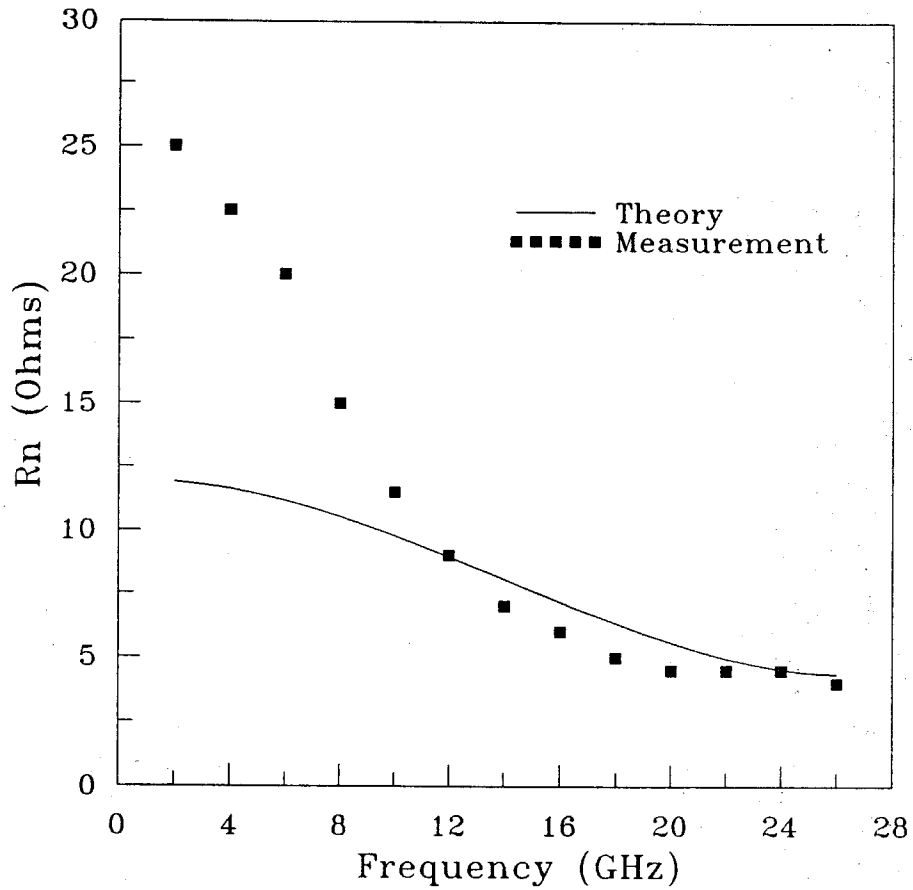
Figure 4.12 Comparison of theory and measurement of the noise resistance R_n for the Fujitsu FHR02X HEMT. The theoretical plot was made with $T_d = 1100$ K.

References

[1] S.W. Wedge and D.B. Rutledge, "Noise waves and passive linear multi-ports," *IEEE Microwave Guided Wave Lett.*, vol. MGL-1, pp. 117-119, May 1991.

[2] R.Q. Twiss, "Nyquist's and Thevenin's theorems generalized for nonreciprocal linear networks," *J. Appl. Phys.*, vol. 26, pp. 599-602, May 1955.

[3] H. Bosma, "On the theory of linear noisy systems," *Philips Res. Repts. Suppl.*, no. 10, 1967.

[4] T.T. Ha, *Solid-State Microwave Amplifier Design*, John Wiley, New York, 1981.

[5] R. Compton, S. W. Wedge, and D. Rutledge, *PUFF: Computer-Aided Design for Microwave Integrated Circuits, Version 1.5*, published at Caltech, Pasadena, California, Jan. 1990.

[6] S. W. Wedge, R. Compton, and D. Rutledge, *PUFF: Computer-Aided Design for Microwave Integrated Circuits, Version 2.0*, software and manual in preparation.

[7] W.J. Getsinger, "Microstrip dispersion model," *IEEE Trans. Microwave Theory Tech.*, vol. MTT-21, pp. 34-39, Jan. 1973.

[8] W.J. Getsinger, "Dispersion of parallel-coupled microstrip,"*IEEE Trans. Microwave Theory Tech.*, vol. MTT-21, pp. 144-145, Mar. 1973.

[9] M. Kirschning and R.H. Jansen, "Accurate model for effective dielectric constant of microstrip with validity up to millimeter wave frequencies," *Electron. Lett.*, vol. 18, pp. 272–273, Mar. 1982.

[10] M. Kirschning and R.H. Jansen, "Accurate wide-range design equations for the frequency dependent characteristics of parallel coupled microstrip lines," *IEEE Trans. Microwave Theory Tech.*, vol. MTT-32, pp. 83-90, Jan. 1984. Corrections: *IEEE Trans. Microwave Theory Tech.*, vol. MTT-33, p. 288, Mar. 1985.

[11] B. Bianco, A. Chiabrera, M. Granara, and S. Ridella, "Frequency dependence of microstrip parameters," *Alta Freq.*, vol. 43, pp. 413-416, July 1974.

[12] E.O. Hammerstad and F. Bekkadal, *A Microstrip Handbook*, ELAB Report, STF 44 A74169, N7034, University of Trondheim, Norway, 1975.

[13] R.A. Pucel, D.J. Masse, and C.P. Hartwig, "Losses in microstrip," *IEEE Trans. Microwave Theory Tech.*, vol. MTT-16, pp. 342–350, June 1968.

[14] K.C. Gupta, R. Garg, and I.J. Bahl, *Microstrip Lines and Slotlines*, Artech House, Dedham, Mass., 1979.

[15] R. Garg and I.J. Bahl, "Characteristics of coupled microstriplines," *IEEE Trans. Microwave Theory Tech.*, vol. MTT-27, pp. 700-705, July 1979.

[16] E. Hammerstad and O. Jensen, "Accurate models for microstrip computer-aided design," *IEEE MTT-S Int. Microwave Symp. Dig.* (Washington, D.C.), pp. 407-409, 1980.

[17] H.A. Wheeler, "Formulas for the skin effect," *Proc. IRE*, vol. 30, pp. 412-424, Sept. 1942.

[18] M.V. Schneider, "Dielectric loss in integrated microwave circuits," *BSTJ*, vol. 48, pp. 2325-2332, Sept. 1969.

[19] B. Ramo Rao, "Effect of loss and frequency dispersion on the performance of microstrip directional couplers and coupled line filters," *IEEE Trans. Microwave Theory Tech.*, vol. MTT-22, pp.747-750, July 1974.

[20] R.E. Collin, *Field Theory of Guided Waves*, IEEE Press, New York, 1991.

[21] A. Cappy, "Noise modeling and measurement techniques," *IEEE Trans. Microwave Theory Tech.*, vol. MTT-36, pp. 1-9, Jan. 1988.

[22] H. Fukui, "Optimal noise figure of microwave GaAs MESFET's," *IEEE Trans. Electron Devices*, vol. ED-26, pp. 1032-1037, July 1979.

[23] A.F. Podell, "A functional GaAs FET noise model," *IEEE Trans. Electron Devices*, vol. ED-28, pp. 511-517, May 1981.

[24] M.S. Gupta, O. Pitzalis, S.E. Rosenbaum, and P.T. Greiling, "Microwave noise characterization of GaAs MESFET's: evaluation by on-wafer low-frequency output noise current measurement," *IEEE Trans. Microwave Theory Tech.*, vol. MTT-35, pp. 1208-1218, Dec. 1987.

[25] M.W. Pospieszalski, "Modeling of noise parameters of MESFET's and MODFET's and their frequency and temperature dependence," *IEEE Trans. Microwave Theory Tech.*, vol. MTT-37, pp. 1340-1350, Sept. 1989.

Chapter 5

Noise Wave Measurement

To make use of the analysis methods developed in chapter 3, the noise wave correlation matrix for each component must be determined. For passive components, or microwave transistors represented by equivalent circuits, the methods of chapter 4 may be employed. When these methods are inappropriate, noise parameters may be found from direct measurement.

The standard technique for two-port noise parameter extraction is to measure the variation in noise figure F as a function of source reflection coefficient Γ_s. The variation follows

$$F = F_{min} + 4\frac{R_n}{Z_0}\frac{|\Gamma_s - \Gamma_{opt}|^2}{|1 + \Gamma_{opt}|^2(1 - |\Gamma_s|^2)} \tag{5.1}$$

and it is therefore possible to solve for noise parameters F_{min}, Γ_{opt}, and R_n. These parameters may be converted to a two-port noise wave correlation matrix using the formulas given in chapter 2. This is referred to as the tuner method, since a tuner is required to generate values of Γ_s.

The wave interpretation of noise suggests a new approach. As mentioned in the derivation of Bosma's theorem (chapter 4), it is possible to measure the correlation of noise waves using directional couplers. This knowledge, combined with simple noise power measurement steps, makes possible the direct measurement of the noise wave correlation matrix.

5.1 Tuner Extraction of Noise Parameters

The apparatus for carrying out noise parameter extraction using the tuner method is shown in Fig. 5.1. A tuner at the input of the device-under-test (DUT) generates reflection coefficient Γ_s. The noise source is otherwise matched to Z_0. A low-noise amplifier (LNA) is used to boost the noise signals, and a mixer and local oscillator downconvert the noise to a lower frequency to allow a radiometric measurement to be made by the noise figure meter. Determination of noise figure is made by making measurements with the noise source at equivalent hot and cold temperatures. Associated gain of the device may also be found using a second tuner at the output of the DUT.
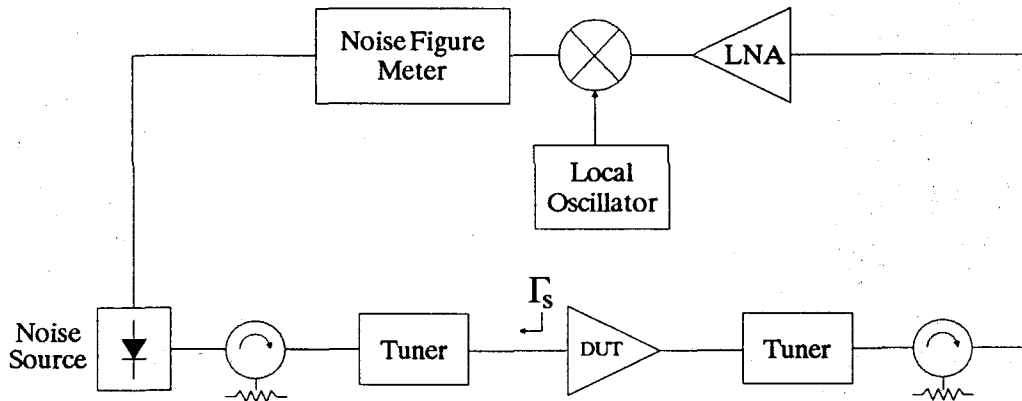

Figure 5.1 Tuner method for noise parameter extraction. One tuner is used to generate the reflection coefficient Γ_s seen at the input of the device-under-test (DUT). At the DUT output, a second tuner is often used to find the associated gain.

Tuning procedures to solve for the noise parameters have been debated for some time. The standard approach [1] is to adjust the tuner until the best noise figure is obtained. The tuner is then removed from the system and the Γ_s generated is measured using a network analyzer. This gives both Γ_{opt} and

F_{min}. By then making an additional noise figure measurement at $\Gamma_s = 0$ and applying (5.1), a value for R_n is determined. Lane [2] pointed out that this method could be inaccurate. He argued that the partial derivative of F was zero at F_{min}, and that it was therefore difficult to pinpoint Γ_{opt}. He advocated multiple measurements of F at various Γ_s values and then a least-squares fit to (5.1). However, application of this technique was found to often result in erroneous results. A host of various procedures then surfaced [3-6], all basically recommending that data for the least squares fit be taken in the vicinity of Γ_{opt}.

There are problems with the tuners themselves. Each has loss, and repeatability errors. Mechanical tuners must be precision machined and have micrometer adjustments to reduce these problems. Even then, each tuner setting must be characterized with full two port measurements to allow removal of tuner introduced errors [7]. Electronic tuners offer a tremendous speed advantage over their mechanical counterparts and permit automatic characterization of devices. However, they generate discrete values in a restricted range for Γ_s, and applying the required least squares fit to the derived data often gives meaningless results. The electronic tuners also require frequent calibration, have a limited frequency range, are lossy, and can cause low frequency oscillations in some microwave transistors [8].

5.2 One-Port Noise Wave Measurements

In section 2.5 it was shown that the measurement of noise figure at $\Gamma_s = 0$ could be related to the noise wave c_2 by

$$F = 1 + \frac{\overline{|c_2|^2}}{kT_0|s_{21}|^2}. \qquad (5.2)$$

The value of the gain $|s_{21}|^2$ also results from the noise figure measurement process, suggesting that it is possible to derive noise wave values from noise figure measurements taken with $\Gamma_s = 0$. This would be a great advantage. Microwave measurements of scattering parameters are performed under these conditions, leading to stability and accuracy. However, (5.2) gives only one value in the noise wave correlation matrix. Modifications must be made based on rethinking the measurement process in terms of noise waves. The first step is to consider a one-port noise wave measurement.

By folding the apparatus of Fig. 5.1 upon itself, the system of Fig. 5.2 is realized. As with the noise figure measurement, the noise source is capable of taking on two equivalent temperatures. A circulator is used to inject the noise from the source into the one-port and to terminate noise originating in the LNA. The one-port reflects some of the noise from the source, and adds its own noise. These combine to form noise wave d. Since the noise source and c will be uncorrelated, the power in d is given by

$$\overline{|d|^2} = \overline{|c|^2} + kT_1|s|^2. \qquad (5.3)$$

By making measurements of $\overline{|d|^2}$ at two known values of T_1, values for both $\overline{|c|^2}$ and $|s|^2$ may be derived. In order to account for system noise, calibrations are made with $|s| = 1$ and $|s| = 0$. This procedure was followed to produce the graph of Fig. 5.3. Noise spectral density measurements were made using a slide screw tuner to generate various values of s. These values were later measured on an HP8510 network analyzer. The measured noise waves are shown compared

to the theory that $\overline{|c|^2} = kT_0(1 - |s|^2)$. The measurement plot is derived from network analyzer values of $|s|$, and $\overline{|c|^2}$ values from the noise wave measurement. The differences shown are therefore due to compounded errors in both $|s|^2$ and $\overline{|c|^2}$. The errors are small, and are most likely due to inaccurate estimates of the noise source temperatures.
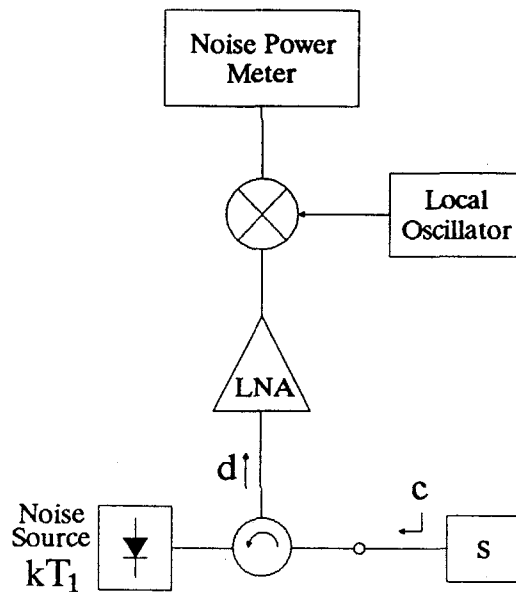

Figure 5.2 Measurement apparatus for a one-port noise wave measurement. Noise wave c emanates from the one-port termination with scattering parameter s. The noise source with power kT_1 generates hot and cold equivalent temperatures.
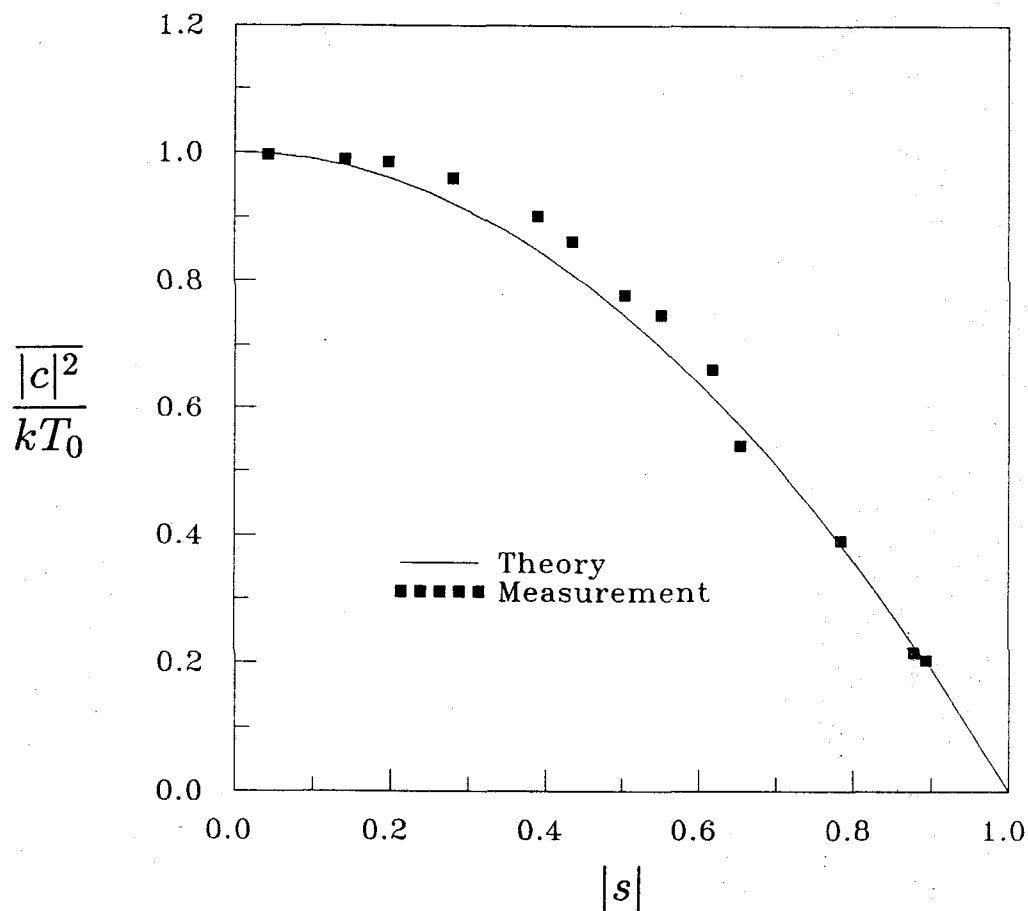
Figure 5.3 Theory compared to noise wave measurements for a one-port. The values of $|s|$ were generated using a slide screw tuner, and measured on an HP8510 network analyzer. The normalized noise wave power $\overline{|c|^2}/kT_0$ is shown compared to the theory that $\overline{|c|^2}/kT_0 = (1 - |s|^2)$.

5.3 Two-Port Noise Wave Measurement

The instrumentation used for the one-port measurement can be extended to the two-port case. Given in Fig. 5.4 is a two-port with scattering matrix S with noise injected at both of its terminals. Noise waves c_1 and c_2 emanate from the network and combine with scattered noise from the sources to produce noise waves d_1 and d_2 given by

$$d_1 = c_1 + \sqrt{kT_1}s_{11} + \sqrt{kT_2}s_{12} \qquad (5.4a)$$

$$d_2 = c_2 + \sqrt{kT_1}s_{21} + \sqrt{kT_2}s_{22}. \qquad (5.4b)$$

These waves will have measurable power densities

$$\overline{|d_1|^2} = \overline{|c_1|^2} + kT_1|s_{11}|^2 + kT_2|s_{12}|^2 \qquad (5.5a)$$

$$\overline{|d_2|^2} = \overline{|c_2|^2} + kT_1|s_{21}|^2 + kT_2|s_{22}|^2. \qquad (5.5b)$$

Four measurements are made of both $\overline{|d_1|^2}$ and $\overline{|d_2|^2}$ using two values for each T_1 and T_2. Sufficient information therefore exists to solve for the six unknowns $\overline{|c_1|^2}$, $\overline{|c_2|^2}$, $|s_{11}|^2$, $|s_{12}|^2$, $|s_{21}|^2$, and $|s_{22}|^2$.

The above measurement gives no information concerning the noise correlation $\overline{c_1 c_2^*}$. As discussed in the derivation of Bosma's theorem, directional couplers are used for this purpose. Shown in Fig. 5.5 is the measurement system of Fig. 5.4 with a directional coupler inserted at a point prior to the noise power measurement. With a lossless $0°/180°$ 3 dB hybrid, the noise waves that exit are given by

$$e_1 = \frac{1}{\sqrt{2}}(d_1 + d_2) \qquad (5.6a)$$

$$e_2 = \frac{1}{\sqrt{2}}(d_1 - d_2). \qquad (5.6b)$$

The noise power measurement will give the following values for $\overline{|e_1|^2}$ and $\overline{|e_2|^2}$

$$\overline{|e_1|^2} = \frac{1}{2}\left[\overline{|d_1|^2} + \overline{|d_2|^2} + 2Re(\overline{d_1 d_2^*})\right] \qquad (5.7a)$$
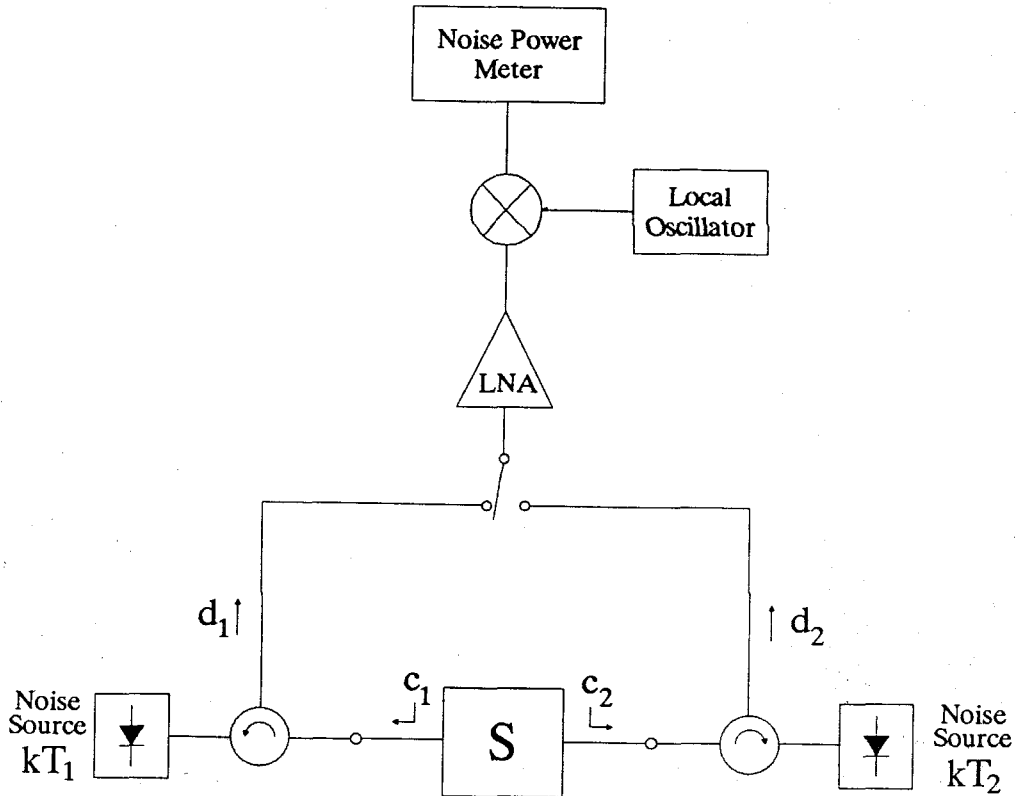
Figure 5.4 Measurement apparatus for the two-port wave measurement of $\overline{|c_1|^2}$ and $\overline{|c_2|^2}$. Noise waves c_1 and c_2 emanate from the network with scattering matrix S. Two noise sources are used with equivalent temperatures T_1 and T_2, each capable of taking on hot and cold values. The switch shown is a non-reflective microwave type.

$$\overline{|e_2|^2} = \tfrac{1}{2}\left[\overline{|d_1|^2} + \overline{|d_2|^2} - 2Re(\overline{d_1 d_2^*})\right]. \tag{5.7b}$$

Taking the difference in these measured power levels yields

$$
\begin{aligned}
\overline{|e_1|^2} - \overline{|e_2|^2} &= 2Re(\overline{d_1 d_2^*}) \\
&= 2\left[Re(\overline{c_1 c_2^*}) + kT_1 Re(s_{11}s_{21}^*) + kT_2 Re(s_{12}s_{22}^*)\right]
\end{aligned}
\tag{5.8}
$$

where consistent values of T_1 and T_2 have been used in the comparison. Solutions for unknowns $Re(\overline{c_1 c_2^*})$, $Re(s_{11}s_{21}^*)$, and $Re(s_{12}s_{22}^*)$ are then found by performing such comparisons for different values of T_1 and T_2.

Next, the 0°/180° hybrid is replaced with a 90° 3 dB hybrid, positioned in the same location of Fig. 5.5. The noise waves at the coupler output are then given by

$$e_1 = \tfrac{-j}{\sqrt{2}}(d_1 + jd_2) \tag{5.9a}$$

$$e_2 = \tfrac{1}{\sqrt{2}}(d_1 - jd_2). \tag{5.9b}$$

Taking the difference in powers now results in

$$
\begin{aligned}
\overline{|e_1|^2} - \overline{|e_2|^2} &= 2Im(\overline{d_1 d_2^*}) \\
&= 2\left[Im(\overline{c_1 c_2^*}) + kT_1 Im(s_{11}s_{21}^*) + kT_2 Im(s_{12}s_{22}^*)\right].
\end{aligned}
\tag{5.10}
$$

Measurements at two values for T_1 and T_2 give the imaginary components, which when combined with the result of (5.8) provide solutions for the three complex quantities $\overline{c_1 c_2^*}$, $s_{11}s_{21}^*$, and $s_{12}s_{22}^*$.

This technique of two-port noise measurement shall be referred to as the *wave method*. It not only measures all values for the noise wave correlation matrix, but also gives the magnitude of the four scattering parameters and the complex quantities $s_{11}s_{21}^*$ and $s_{12}s_{22}^*$. As in the case of the one-port, it is possible to remove noise contributions from the apparatus by following a simple calibration procedure. In addition, the system of equations that is manipulated is typically over-determined, and lends itself to statistical analysis.
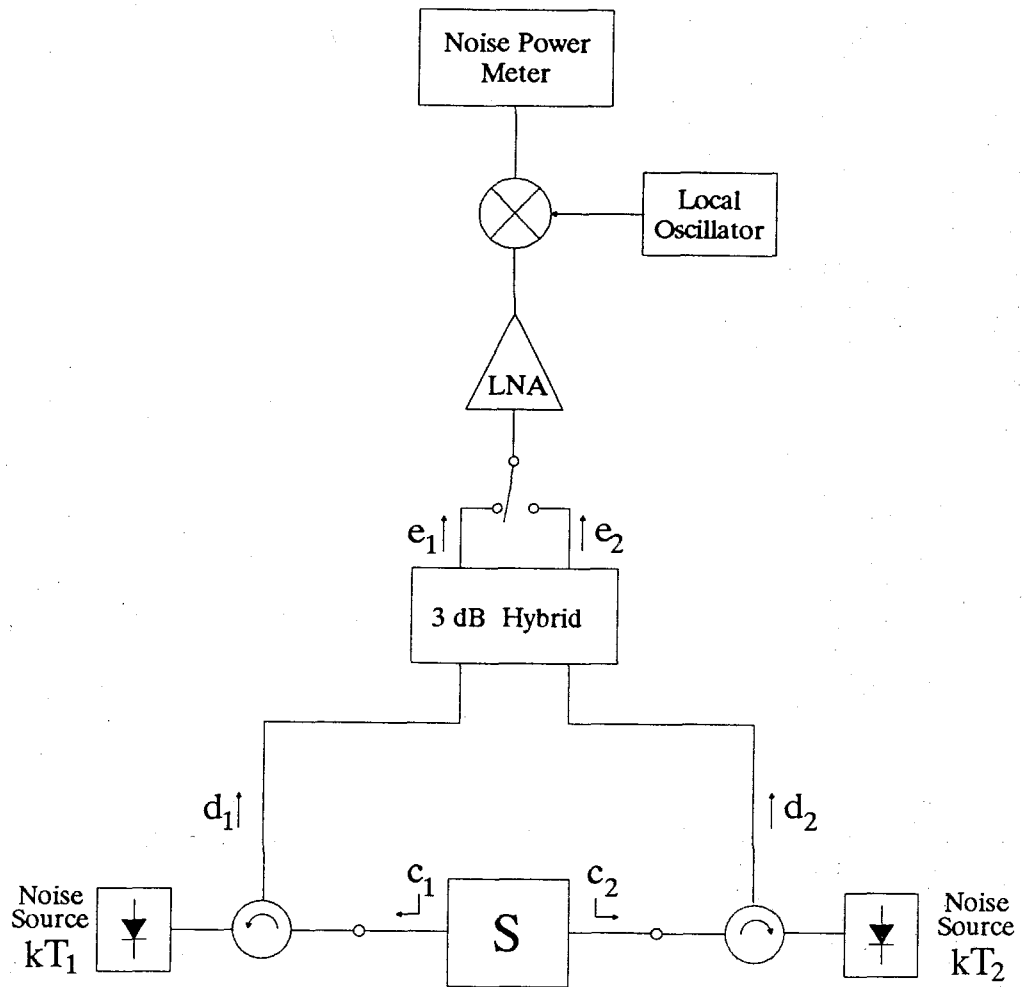
Figure 5.5 A 3 dB hybrid coupler inserted into the measurement apparatus of Fig. 5.4. A 0°/180° coupler allows measurement of $Re(\overline{c_1 c_2^*})$, while a 90° coupler allows measurement of $Im(\overline{c_1 c_2^*})$.

In order to evaluate the wave method, a system was constructed for operation at 4 GHz. A simple calibration procedure was used, and a series of measurements were made on a GaAs FET amplifier over a range of bias currents. For comparison, measurements were made at the same bias points using the tuner method described previously. A mechanical slide screw tuner was used and the additional measurements and corrections recommended by Strid [7] were performed. For compatibility, the results are compared in terms of standard noise parameters. Presented in Fig. 5.6 are the results for $|\Gamma_{opt}|$ shown on an enlarged scale. Agreement over most of the range is within 0.05. Some of this disparity is due to lack of repeatability in the tuner. The results for F_{min} are given in Fig. 5.7. The total uncertainty in the noise figure measurement is 0.25 dB, and the majority of the data falls in this range. Data for R_n are shown in Fig. 5.8, and the behavior of the two plots over bias current is very similar.

The agreement between the three comparisons is remarkable considering the differences in the measurement methods. It is impossible, in fact, to specify which of the plots are "correct." Measurements made with the tuner method, in addition to its aforementioned problems, were seen to cause unstable bias conditions. These have no doubt contributed to some of the errors. In the application of the wave method, uncertainty in temperatures T_1 and T_2 could have led to errors. One point is clear. The wave method has a considerable number of advantages. It does not require network analyzer calibration and does not have "moving parts" as in the case of the mechanical tuner. Since the device-under-test is always presented with impedance Z_0, the measurement process is much more stable. The networks used for measuring correlation are simple, and can be constructed with off-the-shelf components. They are also available into millimeter-wave frequencies, whereas mechanical and electronic tuners are currently limited to 18 GHz operation. The wave method also provides scattering parameter information equivalent to a scalar network analyzer.
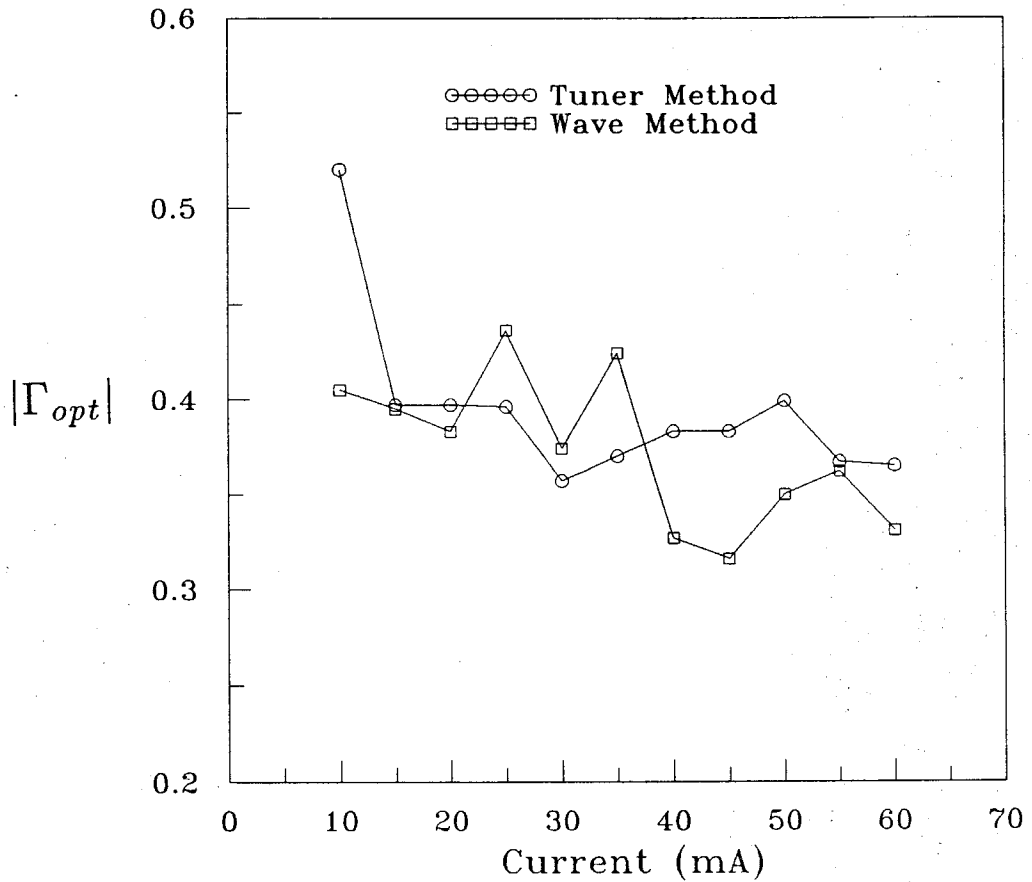
Figure 5.6 Comparison of the tuner and wave measurement methods for determining the optimum reflection coefficient Γ_{opt} for a GaAs FET amplifier. The measurements were performed at 4 GHz with amplifier bias current varied from 10-60 mA.
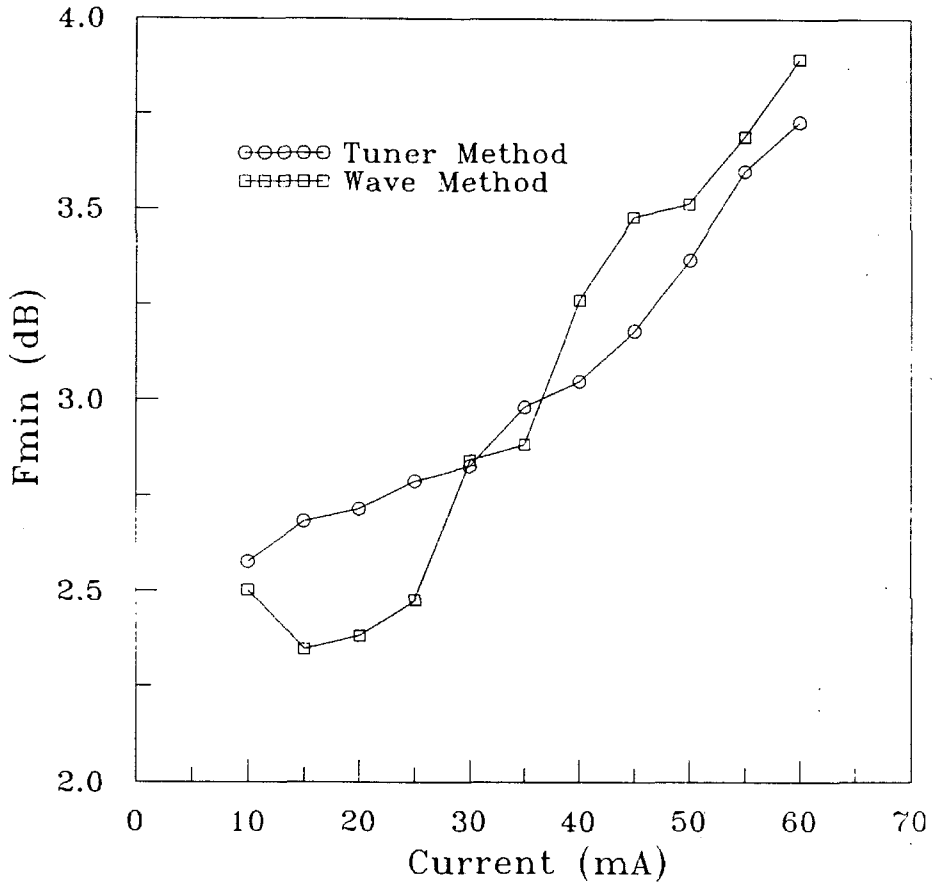
Figure 5.7 Comparison of tuner and wave measurement methods for determining the noise figure minimum F_{min} for a GaAs FET amplifier at 4 GHz with varying bias current.
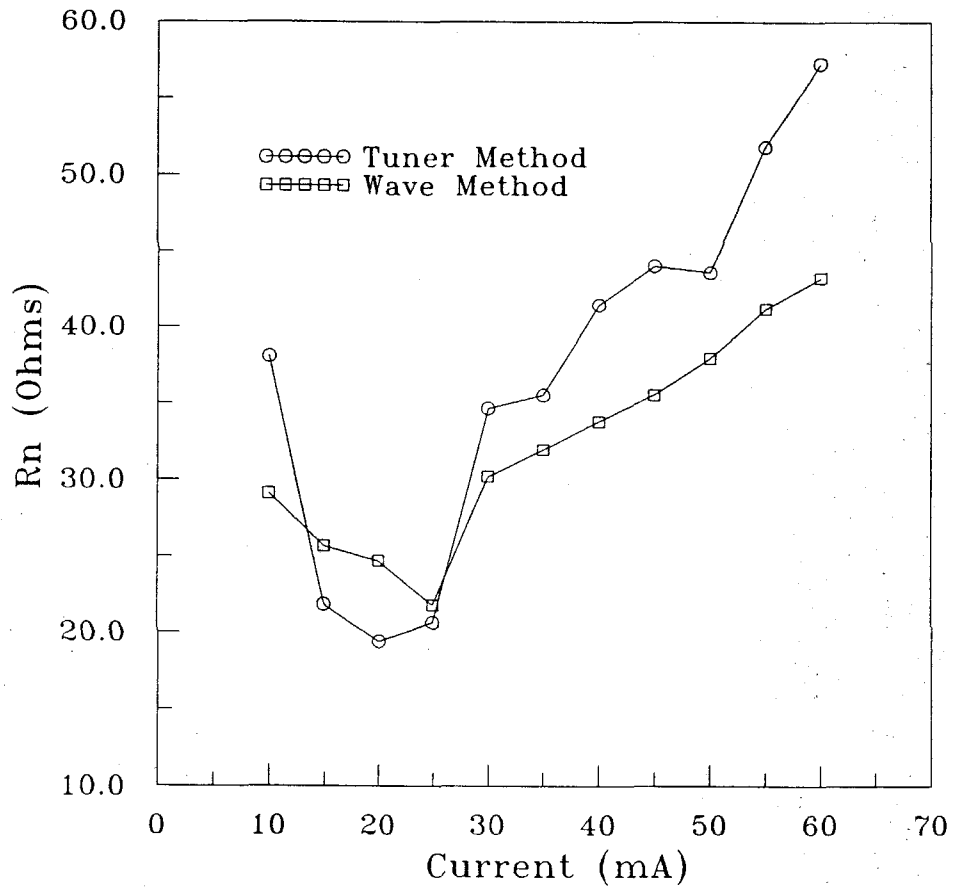
Figure 5.8 Comparison of the tuner and wave measurement methods for determining the noise resistance R_n for a GaAs FET amplifier at 4 GHz with varying bias current.

References

[1] IRE Subcommittee on Noise, "IRE standards on methods of measuring noise in linear twoports, 1959," *Proc. IRE*, vol. 48, pp. 60-68, Jan. 1960.

[2] R.Q. Lane, "The determination of device noise parameters," *Proc. IEEE*, vol. 57, pp. 1461-1462, Aug. 1969.

[3] W. Kokyczka, A. Leupp, and M.J.O. Strutt, "Computer–aided determination of two-port noise parameters (CADON)," *Proc. IEEE*, vol. 58, pp. 1850-1851, Nov. 1970.

[4] G. Caruso and M. Sannino, "Computer–aided determination of microwave two–port noise parameters," *IEEE Trans. Microwave Theory Tech.*, vol. MTT-26, pp. 639-642, Sept. 1978.

[5] M. Mitama and H. Katoh, "An improved computational method for noise parameter measurement," *IEEE Trans. Microwave Theory Tech.*, vol. MTT-27, pp. 612-615, June 1979.

[6] M. Sannino, "On the determination of device noise and gain parameters," *Proc. IEEE*, vol. 67, pp. 1364-1366, Sept. 1979.

[7] E.W. Strid, "Measurement of losses in noise–matching networks," *IEEE Trans. Microwave Theory Tech.*, vol. MTT-29, pp. 247–252, Mar. 1981.

[8] A. Cappy, "Noise modeling and measurement techniques," *IEEE Trans. Microwave Theory Tech.*, vol. MTT-36, pp. 1-10, Jan. 1988.

Chapter 6

Conclusions and Suggestions for Future Work

The wave approach has been shown to be a powerful means for the character-
ization and analysis of noise in microwave circuits. It permits scattering matrix
and signal-flow graph theory to be used for noise calculations, simplifying the
microwave computer-aided design process. Derivation of the noise wave proper-
ties for many microwave components is a straightforward process, requiring only
scattering parameters and device temperature. The wave approach has also led
to new measurement techniques that offer advantages over current methods and
yield comparable results.

Although many theoretical aspects of computer-aided noise analysis have
been considered here, there is still considerable work to be done in the area.
Only linear methods have been discussed, but many nonlinear circuits require
noise analysis, as well. Successful methods have been developed to specifically
analyze noise in nonlinear microwave diode mixers [1,2], yet more general anal-
ysis techniques are needed. Some promising new methods have recently been
proposed [3].

Improved noise modeling of components is also in demand. The models
presented here have given good results, but they are based on bias dependent
equivalent circuits. Needed are expressions that relate the equivalent tempera-
tures used in GaAs FET and HEMT models to bias and device properties. It was
Podell [4] who first demonstrated that this could be done, yet his models must

be upgraded to include the effects of correlated noise. Noisy nonlinear transistor models are also needed to accompany new nonlinear analysis methods [5]. Further work in the area of passive circuit modeling is also needed. In chapter 4, methods were discussed for modeling dielectric and conductor losses and surface roughness effects. Not considered, although important in some circuits, are noise contributions due to radiation loss.

The promise of the wave method for noise parameter extraction needs to be exploited. The method discussed in chapter 5 requires the swapping of directional couplers. Preferred is a single network that allows parameter extraction from noise power measurements at its outputs. This is possible using the six-port network described by Engen [6]. This network has been used successfully to make accurate scattering parameter measurements. It may also be used for noise-parameter measurements. A potential measurement system is shown in Fig. 6.1. The six-port network consists of three 90° 3-dB quadrature hybrids (each denoted by a 'Q'), and a single 180° 3-dB coupler (denoted by an 'H'). When two input noise waves d_1 and d_2 are incident on the network, the output powers P_1–P_4 are given by:

$$P_1 = \overline{\left| \tfrac{1}{\sqrt{2}} d_1 - \tfrac{i}{2} d_2 \right|^2} \tag{6.1a}$$

$$P_2 = \overline{\left| \tfrac{-i}{2} \left[d_1 + \tfrac{1+i}{\sqrt{2}} d_2 \right] \right|^2} \tag{6.1b}$$

$$P_3 = \overline{\left| \tfrac{-i}{2} \left[d_1 - \tfrac{1-i}{\sqrt{2}} d_2 \right] \right|^2} \tag{6.1c}$$

$$P_4 = \overline{\left| \tfrac{-i}{2} d_2 \right|^2}. \tag{6.1d}$$

Comparison of these power measurements gives

$$\overline{|d_1|^2} = P_1 + P_2 + P_3 - 3P_4 \tag{6.2a}$$

$$\overline{|d_2|^2} = 4P_4 \tag{6.2b}$$

$$Re(\overline{d_1 d_2^*}) = \sqrt{2}(P_2 - P_3) \qquad\qquad (6.2c)$$

$$Im(\overline{d_1 d_2^*}) = \tfrac{1}{\sqrt{2}}(P_2 - P_1 + P_3 - P_4). \qquad\qquad (6.2d)$$

By making measurements at two noise source temperatures, and employing the methods described in chapter 5, it is possible to derive the noise wave correlation matrix for the device-under-test, as well as substantial scattering parameter information.
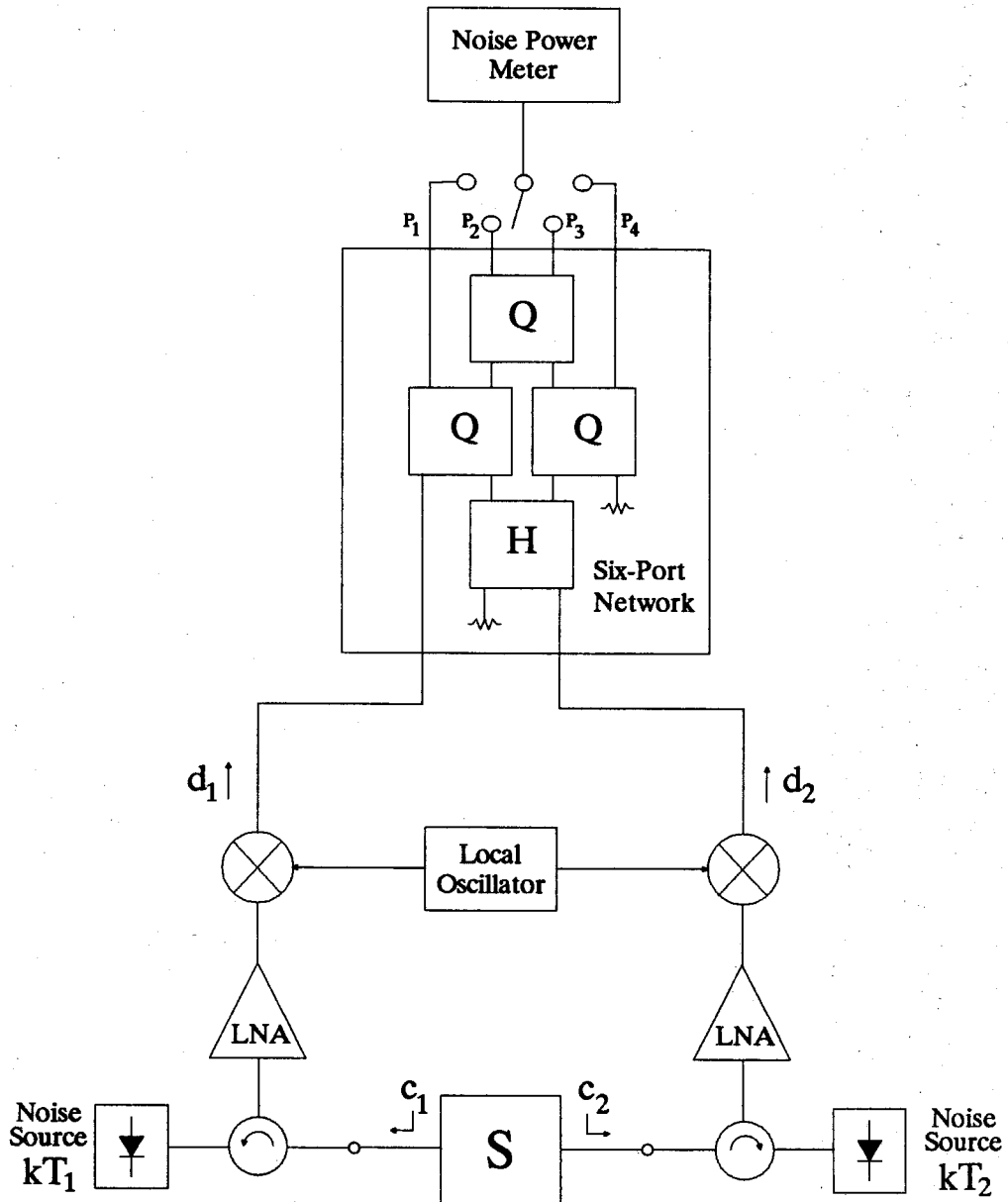
Figure 6.1 A noise parameter analyzer using a six-port circuit. The components of the six-port are a single 0°/180° 3 dB hybrid coupler, labeled as **H**, and three 90° 3 dB quadrature hybrids, each labeled as **Q**. The six-port shown operates at an intermediate frequency.

References

[1] D.N. Held and A.R. Kerr, "Conversion loss and noise of microwave and millimeter-wave mixers: Part 1–Theory," *IEEE Trans. Microwave Theory Tech.*, vol. MTT-26, pp. 49–55, Feb. 1978.

[2] A.R. Kerr, "Noise and loss in balanced and subharmonically pumped mixers: Part 1–Theory," *IEEE Trans. Microwave Theory Tech.*, vol. MTT-27, pp. 938-943, Dec. 1979.

[3] V. Rizzoli and A. Neri, "State of the art and present trends in nonlinear microwave CAD techniques," *IEEE Trans. Microwave Theory Tech.*, vol. MTT-36, pp. 343-365, Feb. 1988.

[4] A.F. Podell, "A functional GaAs FET noise model," *IEEE Trans. Electron Devices*, vol. ED-28, pp. 511-517, May 1981.

[5] V. Rizzoli, F. Mastri, and C. Cecchetti, "Computer-aided noise analysis of MESFET and HEMT mixers," *IEEE Trans. Microwave Theory Tech.*, vol. MTT-37, pp. 1401-1410, Sept. 1979.

[6] G.F. Engen, "An improved circuit for implementing the six-port technique of microwave measurements," *IEEE Trans. Microwave Theory Tech.*, vol. MTT-25, pp. 1080-1083, Dec. 1977.